A Dissertation for the Degree of Ph.D. in Engineering

Tracking and Fast Handover Mechanisms Using Station Identification for Ground-to-Train Free-Space Optical Communication

March 2023

Graduate School of Science and Technology,
Keio University

Kosuke Mori

Abstract

Users' demands for using the Internet in a high-speed train have been increasing in recent years. Although mobile terminals such as cellular phones are available for the passengers in a train, it is better to provide a high-speed train with a broadband communication link to the Internet and Wi-Fi communication is provided to the passengers. Existing ground-to-train communication technologies, such as leaky coaxial cables, Wi-Fi, WiMAX, and LTE-R, have throughput of tens of hundreds Mbps while the required throughput to a high-speed train will reach 11-35 Gbps by 2030. Even in research using millimeter waves for communication with mobile vehicles, the current throughput is less than 10 Gbps. To meet the demands of broadband ground-to-train communication, free-space optical communication technology has attracted significant attention. With this technology, a mobile station installed on a train communicates with one of the ground stations installed along the railway as both stations track each other while the mobile station performs handovers to switch the correspondent ground station as the train runs. In one of the existing proposals, a laser communication system called LaserTrainComm2012 (LTC12) was developed. LTC12 employs a beacon beam and a mirror actuator to track the communication peer. Since LTC12 cannot precisely detect the location of the beacon light, it repeatedly moves the mirror little by little. The Layer-2 handover time is approximately 40 ms at 60 km/h.

This dissertation has four main contributions. The first contribution is reduction of tracking time in an improved laser communication system called LaserTrainComm2014 (LTC14). LTC14 employs a high-speed camera which enables detecting the position of the beacon light. The combination of rough tracking with camera image recognition and precise tracking with QPD (Quadrant Photo Diode) enables faster and more accurate tracking than that in LTC12. As a result, the Layer-2 handover time is approximately 21 ms at a speed of 60 km/h. LTC14, however, has several problems

such as unstable tracking due to analog control of the mirror actuator, overshooting of mirror actuation due to inertia caused by the large mirror, and inability to identify each LTC14. Thus, a new laser communication system called LaserTrainComm2022 (LTC22) was developed with a 100 Mbps laser communication device. The second contribution is improvement of tracking accuracy and handover speed by employing digitally controlled mirror actuators. The third contribution is stabilization of communication quality just after handover by separating a large mirror into two small mirrors for transmission and reception, respectively. The final contribution is identification of each LTC22 with station ID, which is encoded and modulated into the beacon light with 2PPM (Pulse Position Modulation). As a result, LTC22 correctly detects the communication peer at handover. The rough and precise tracking is performed with a dual-port camera capable of simultaneously acquiring wide and narrow images. The blinking of the beacon light is controlled so that the intensity of the beacon light can be detected in the wide image and the station ID can be detected in the narrow image. Layer-2 (L2) handover time and TCP throughput during handover were measured in a test course for vehicles. A LTC22 was installed on a car as a mobile station and two LTC22s were installed on the road at a distance of 30 m as the ground stations. At 40 km/h, the handover time is approximately 1 ms. The TCP throughput is approximately 94 Mbps before and after handover and only dropped to 75-77 Mbps during handover. Analysis results show that tracking and handover are possible even at a speed of 300 km/h or 500 km/h. Since the handover time is not affected by the link rate of a communication device, the handover time will be 1 ms even if the link rate of communication device is 10 Gbps or higher.

Acknowledgments

Firstly, I am expressing my sincere gratitude to Prof. Fumio Teraoka He guided me carefully as my supervisor for a long time and is the chair of my dissertation committee. I also appreciate Prof. Shinichiro Haruyama, who collaborated with me on my doctoral dissertation and is the vice-chair of my dissertation committee. I take pride in my involvement in the LaserTrain-Comm project. I would like to express my gratitude to the vice-chairs of my dissertation committee: Assoc. Prof. Kunitake Kaneko and Prof. Hiroshi Shigeno.

I would like to extend my thanks to Ryoji Murakami, Xiao Yu, Yohei Hoashi (the Haruyama Lab), Masanori Terada, Komei Shimamura, Yuki Nagai, and Rempei Sawada (the Teraoka Lab) for helping me to conduct experiments at the Keio Shin-Kawasaki Town Campus and the test courses. I would also like to thank Takefumi Miyoshi of WasaLab, LLC. for his assistance in developing the system on the FPGA board of LTC22. I am grateful for the collaboration with ITRI (Industrial Technology Research Institute) and thank Ruei-Bin Chen from ITRI, who worked with me at the Keio Yagami Campus for a couple of months.

Furthermore, I appreciate the courtesies of Toyo Electric Corporation, Hamamatsu Photonics K.K., and Stanley Electric Co. which allowed us to use their trial products for LTC14 and LTC22. I would also like to thank "Japan Construction Method and Machinery Research Institute" and JARI (Japan Automobile Research Institute) for allowing us to use their test courses.

While it is difficult to mention them all by name, I also thank the members of my laboratory.

Finally, I would like to express my sincere gratitude to my family.

Contents

Abstract **i**

Acknowledgments **iii**

List of Figures **ix**

List of Tables **x**

1 Introduction **1**
- 1.1 Background 1
- 1.2 Ground-to-Train Communication Technologies 2
- 1.3 Existing Ground-to-Train Free Space Communication Technology 4
- 1.4 Contributions of this Dissertation 6
- 1.5 Structure of this Dissertation 7

2 Related Work **8**
- 2.1 Communication Methods for Train Network 8
- 2.2 Free-Space Optical Communication 9
- 2.3 LaserTrainComm2012 11
  - 2.3.1 Overview 11
  - 2.3.2 Two-Dimensional Mirror Control 12
  - 2.3.3 Tracking and Handover Mechanism 13
  - 2.3.4 Problems of LaserTrainComm2012 13

3 Rough Tracking by High-Speed Camera (LaserTrainComm2014) 15
3.1 System Design . . . 15
3.1.1 Block Diagram . . . 15
3.1.2 High-Speed Camera . . . 16
3.1.3 Quadrant Photo Diode (QPD) . . . 17
3.1.4 Proximity Sensor . . . 18
3.2 State Transition Diagram . . . 18
3.2.1 Beacon Acquisition . . . 20
3.2.2 Handover . . . 20
3.2.3 Temporal Shadowing . . . 21
3.3 High-Speed Detection and Acquisition of Beacon Light Using Camera . . . 22
3.3.1 Recognition and Labeling of Beacon Light . . . 23
3.3.2 Inter-Frame Label Identification . . . 25
3.4 Evaluation . . . 27
3.4.1 Evaluation Environment . . . 27
3.4.2 Mirror Direction Measurement of Beacon Acquisition and Tracking . . . 27
3.4.3 Disruption Time due to Handover . . . 29
3.5 Problems of LaserTrainComm2014 . . . 33

4 Improved Tracking and Handover Accuracy with Station ID (LaserTrainComm2022) 34
4.1 System Design . . . 34
4.1.1 Block Diagram . . . 35
4.1.2 Dual-Port Camera . . . 36
4.1.3 LED Beacon . . . 37
4.1.4 Mirrors and Mirror Actuators . . . 39
4.1.5 System Controller . . . 40
4.1.6 System Configuration . . . 42
4.2 Coding and Modulation of Station ID . . . 44
4.2.1 Station ID Coding . . . 44
4.2.2 Station ID Modulation . . . 46
4.2.3 Beacon Capturing . . . 49

4.3 Tracking Method 54
4.3.1 State Transition Diagram 54
4.3.2 Beacon Tracking 57
4.3.3 Handover 57
4.4 Evaluation 58
4.4.1 Evaluation Environment 58
4.4.2 Disruption Time due to Handover 59
4.4.3 Throughput during Handover 61

5 Discussion 65
5.1 Suitability for Real Environment 65
5.2 Impact of Demodulation Time 66

6 Conclusion 69

References 72

Appendix 78

A Structure of Control Software for LaserTrainComm2022 78

B Manual of LaserTrainComm2022 81
B.1 ESP32-WROOM-32 Micro Computer 81
B.2 Windows OS 82
B.3 Linux OS on Zynq Board 84

C Measurement of Beacon Light's Observable Range 85

D Calibration 89

E Emulation Environment of Network Mobility 96

F Dealing with Nose in Image of Dual-Port Camera 100

G Dealing with Interference between Communication Light and Beacon Light 102

List of Figures

1.1 Mobile Network Connection Speed Prediction based on [1]. . . 3
1.2 Overview of ground-to-train free-space optical communication system. 5

2.1 Block diagram of LTC12. 11
2.2 QPD output signals before and after handover. 14

3.1 Photo of LaserTrainComm2014 (LTC14). 16
3.2 Block diagram of LTC14). 17
3.3 State transition diagram of LaserTrainComm2014 (LTC14). . 19
3.4 Beacon light images. 22
3.5 Image processing. 23
3.6 Relation between a ground station and a moving mobile station. 25
3.7 Handover experiments of LaserTrainComm2014 (LTC14) using a car. 28
3.8 Experiment setup of LaserTrainComm2014 (LTC14). 29
3.9 Mirror direction, tracking mode, and connectivity for 1 second before and after handover at 30 km/h. 30
3.10 Mirror direction, tracking mode, and connectivity for 1 second before and after handover at 60 km/h. 31
3.11 Mirror direction, tracking mode, and connectivity for 1 second before and after handover at 90 km/h. 32

4.1 LaserTrainComm2022 (LTC22) block diagram. 36
4.2 Wide view and narrow view. 38
4.3 Appearance of mirror actuators in LTC22 40

4.4 Buffer for image transfer (Upper: Buffer. Lower: Detail of a frame block). 41
4.5 System Details. 42
4.6 System appearance 1. 43
4.7 System appearance 2. 43
4.8 Station ID coding. 45
4.9 Station ID frame. 45
4.10 Actual beacon lighting (two patterns). 47
4.11 Beacon light intensity in the wide view image and the narrow view image. 48
4.12 Beacon detection in a wide view. 50
4.13 Frame-by-frame variation of the center of the beacon candidate's intensity. 51
4.14 State Transition Diagram. 56
4.15 Environment at Yagami campus. 60
4.16 Environment at JARI. 61
4.17 Evaluation environment. 62
4.18 Evaluation network. 63
4.19 Result of ping command for 1 seconds around handover at 40 km/h. 63
4.20 Throughput for 3,000 milliseconds around handover at 40 km/h. 64

5.1 An example in which communication is not disrupted. 68

A.1 Structure of source codes of LaserTrainComm2022. 80

C.1 LED beacon light emitters for the measurement of beacon light's observable range. 86
C.2 Dual-port camera for the measurement of beacon light's observable range. 86
C.3 LED beacon light emitters seen from dual-port camera. 87

D.1 3D view of the device. 92
D.2 Vertical actuator rotated θ degrees from Y axis. 93
D.3 Horizontal actuator rotated α degrees from X axis. 93
D.4 (x_c, y_c) and f in the image. 94

D.5 Environment for calibration. 94
D.6 Photo of calibration. 95

E.1 Network mobility environment in ground-to-train communication. 97
E.2 Emulation environment of network mobility. 98
E.3 Result of emulation: Signaling in Layer-3. 99

F.1 Striped noise in a difference image. 101

G.1 Optical spectrum of beacon light. 103
G.2 Optical spectrum of communication light. 104
G.3 Stacked two 900 nm short-pass filter at a 30-degree angle. . . . 104
G.4 Optical spectrum of filtered beacon light. 105
G.5 Optical spectrum of filtered communication light. 105

List of Tables

2.1 Existing train networks. 9
2.2 Specification of the control unit. 12

3.1 Specifications of high-speed camera. 18
3.2 Handover time in Layer-2. 32

4.1 Specifications of dual-port camera. 37
4.2 Specifications of Lens. 37
4.3 Specifications of LED beacons. 38
4.4 Specifications of mirror actuators. 39
4.5 Specifications of optical communication device. 44
4.6 Rules for how to interpret binazied values to HIGH slot(s) or LOW slot(s). 53
4.7 Experimental results. 62

5.1 $\theta_1 - \theta_2$ in various speeds and distance between ground stations. 68

C.1 Experimental result: The intensity of beacon light or noise in the difference image. 88

E.1 Throughput between the mobile node and the correspondent node. 99

Chapter 1

Introduction

1.1 Background

The Internet was originally designed as a wired network. While wireless communication technologies such as ALOHA [2] existed for remote nodes, these technologies did not support communication between mobile nodes. Wireless local area networks (WLANs) such as Wi-Fi subsequently emerged and were integrated into the Internet. Cellular phones also got connectivity to the Internet. As a result, support for host mobility is required because mobile terminals such as smartphones connected to the Internet through Wi-Fi and cellular networks. Moreover, network mobility is required because a group of mobile terminals forms a network, which changes the point of attachment to the Internet, i.e., a mobile network.

For example, there is a demand for network conferencing while traveling on high-speed trains like the Shinkansen. Although cellular phones

can be used in trains, the cellular network become overloaded due to the simultaneous handover of passengers' mobile terminals. For a mobile network in a train, two key technologies are required: (i) high-speed ground-to-train communication technology that supports tracking and handover; (ii) network mobility support protocol in the network layer. Even if a single mobile terminal consumes low bandwidth, high-speed communication is required to a train because there are a lot of passengers' mobile terminals in a train. Since a train is moving, the transceiver on the ground (ground station) and the transceiver on the train (mobile station) must be able to track each other. Furthermore, the mobile station must be able to switch the current ground station to the next one when the train moves beyond the communication range of the current ground station (handover). On the other hand, a network mobility support protocol in the network layer has been standardized as RFC 3963 [3]. Thus, this dissertation focuses on high-speed communication technology that supports tracking and handover.

1.2 Ground-to-Train Communication Technologies

Figure 1.1 shows the throughput of mobile devices in the Pacific Asian region reported by Cisco [1] and the throughput by 2030 predicted by the author. As shown in Fig. 1.1, the throughput per individual will reach 90 Mbps by 2030. Considering that the capacity of a Shinkansen train is approximately 1,300 passengers and that between 10-30% of all passengers use the Internet as the

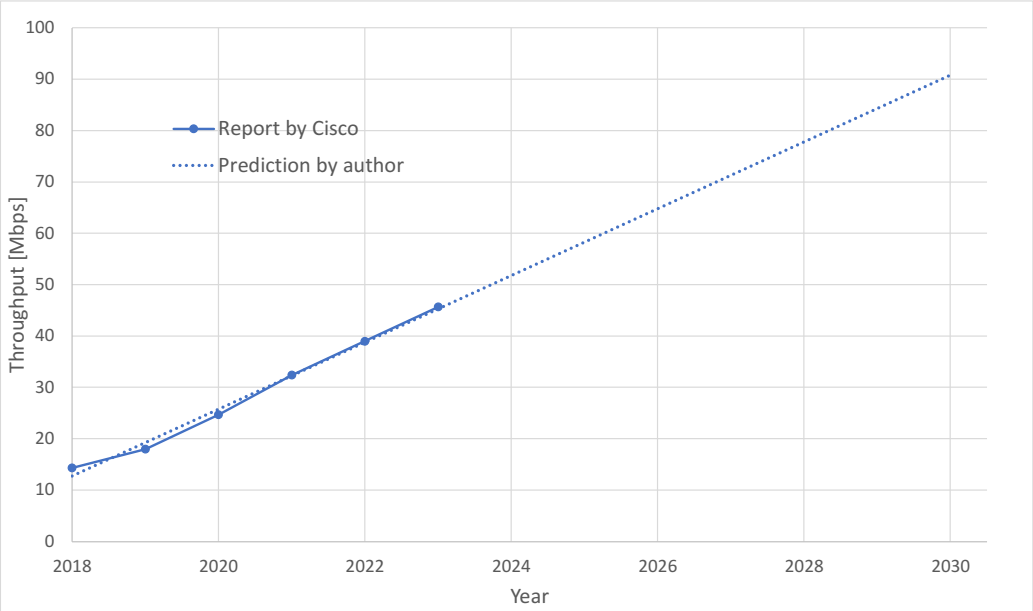

Figure 1.1: Mobile Network Connection Speed Prediction based on [1].

same time, the total throughput for a train would range from 11 Gbps to 35 Gbps. The throughput to be provided to a train will continue to increase as teleconferencing in a train becomes more prevalent.

Although mobile devices such as cellular phones are available for passengers in trains and their throughput is from 100 Mbps to 1 Gbps. The cellular network become overloaded due to the simultaneous handover of passenger's devices. It is better to provide trains with high-speed broadband communication links to the Internet and offer Wi-Fi connectivity to passengers. Existing ground-to-train communication technologies such as leaky coaxial cables, Wi-Fi [4], WiMAX [5], and LTE-R [6] [7] have throughput ranging from tens to hundreds of Mbps. Even in research using millimeter

waves for communication with mobile devices, the current throughput is less than 10 Gbps [8].

Free-space optical communication technology has attracted great attention as a method for achieving high throughput communications exceeding 10 Gbps. This technology uses visible and near-infrared light for communication with frequencies higher than 300 THz, which is higher than the frequencies of radio waves. The throughput of free-space optical communication can reach several tens of Gbps or higher, and it does not require a license like radio wave communication. However, free-space optical communication is highly dependent on line-of-sight and is susceptible to obstacles due to its high frequency.

1.3 Existing Ground-to-Train Free Space Communication Technology

Ground-to-Train Free-Space Optical Communication is proposed to achieve high throughput communication to trains. Figure 1.2 shows an overview of this system. As shown in Fig. 1.2, a mobile station on a train tracks ground stations along the railway. As the train moves, the mobile station handovers to the appropriate ground station. For make this system practical, there are three requirements. First, the communication distance should be at least 300 meters or longer. Because the shape of the Tokaido Shinkansen railway has a significant number of curves, the number of required ground stations

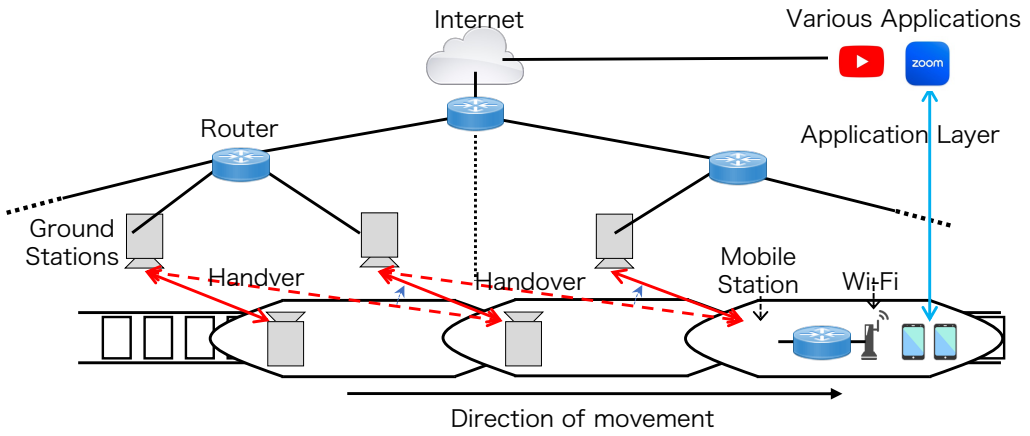

Figure 1.2: Overview of ground-to-train free-space optical communication system.

does not decrease so much even if the distance between ground stations exceeds 300 meters. Second, the system must be able to track and handover at speeds of 300 km/h or 500 km/h assuming that this system will be used on a Shinkansen or linear Shinkansen train. Third, the handover time in Layer-3 should be less than 310 ms [9]. Assuming that the time for Layer-3 handover control is 10-20 ms, the handover time in Layer-2 should be less than 290-300 ms. One of the existing proposals for grand-to-train communication is a laser communication system called *LaserTrainComm2012* (*LTC12*) [10]. Note that "LTCxx" ("xx" is any number) indicates the architecture of the communication system while "LTCxx device" indicates an individual communication device. LTC12 employs a beacon beam and a mirror actuator to track the communication peer and has a Layer-2 handover time of approximately 40 ms at 60 km/h.

1.4 Contributions of this Dissertation

This dissertation aims at providing a high-speed network environment to trains using free-space optical communication that will meet the throughput demands of the future forecasts. This dissertation presents four main contributions. The first contribution is reduction of tracking time in an advanced laser communication system called *LaserTrainComm2014* (*LTC14*) [11] [12] compared with the existing laser communication system called LTC12. Since LTC12 cannot precisely detect the location of the beacon light, it repeatedly moves the mirror little by little. The Layer-2 handover time is approximately 40 ms at 60 km/h. LTC14 combines rough tracking using camera image recognition and precise tracking with QPD (Quadrant Photo Diode) to enable fast and accurate tracking. As a result, the Layer-2 handover time of LTC14 is approximately 21 ms at 60 km/h. However, LTC14 has several problems such as unstable tracking due to analog control of the mirror actuator, overshooting of mirror actuation caused by the large mirror, and lack of identification of each LTC14 device. Thus, a new laser communication system called *LaserTrainComm2022* (*LTC22*) [13] was developed with a 100 Mbps laser communication device. The second contribution is improvement of tracking accuracy and handover speed with digitally controlled mirror actuators. The third contribution is stabilization of communication quality just after handover by separating a large mirror into two small mirrors for transmission and reception. The final contribution is identification of each LTC22 device with a station ID, which is encoded and modulated into the beacon

light using 2PPM (Pulse Position Modulation). As a result, LTC22 correctly detects the communication peer at handover. The rough and precise tracking is performed using a dual-port camera capable of simultaneously acquiring wide and narrow images. The blinking of the beacon light is controlled so that the intensity of the beacon light can be detected in the wide image, and the station ID can be detected in the narrow image.

1.5 Structure of this Dissertation

This dissertation is organized as follows: In Chapter 1, the necessity and requirements for ground-to-train optical communication system are described. In Chapter 2, related works, including existing ground-to-train communication technologies and the existing ground-to-train optical communication system called LTC12, are explained. In Chapter 3, an overview of the LTC14 system, experimental results, and issues are provided. In Chapter 4, LTC22, which improves tracking accuracy and handover precision using station ID, is described. In Chapter 5, the implementation of LTC22 in actual scenarios such as the Shinkansen is discussed. Chapter 6 concludes this dissertation.

Chapter 2

Related Work

2.1 Communication Methods for Train Network

Several methods have been proposed for communication between ground and high-speed trains, including leaky coaxial cables (LCX), Wi-Fi, WiMAX, and 5G (millimeter wave). LCX, Wi-Fi, WiMAX, and LTE are already in practical use. 5G (millimeter wave) is still in the experimental stage [14–17]. The characteristics of these schemes are shown in Table 2.1.

LCX provides stable communication between the LCX and the antennas installed in a vehicle [18] in short and stable distance. Wi-Fi and WiMAX provide wireless broadband access [5] [19].

In recent years, the 5G cellular network has also attracted attention as a network for trains or mobile vehicles [8] [15] [20] [21]. High-speed communication using millimeter-wave (28 GHz band) for high-speed mobile vehicles

Table 2.1: Existing train networks.

Method	Throughput	Remarks
LCX	2 Mbps	Handover does not occur
Wi-Fi	54 Mbps	Communication failure time is less than 1% during handover [4]
WiMax	40 Mbps	Throughput is 0 for several seconds during handover [5]
LTE	75 Mbps	LTE-R [6] [7] is deployed in China. Handover time is not clearly stated
5G (Millimeter Waves)	1 Gbps	Under an experiment. 283 km/h

are proposed. In [15], millimeter-wave communication between a car at 265 km/h and a ground station is tested and achieves the throughput of 2 Gbps. In addition, millimeter wave communication is tested between a ground station and a train running at 283 km/h in [8] and achieves the throughput of 1 Gbps. However, none of them has achieved the throughput of 10 Gbps or higher that can be achieved in free-space optical-space communication.

2.2 Free-Space Optical Communication

Free-space optical communication systems have been proposed for ground-to-ground communication [22]. One of the systems uses laser beams and it is tested the communication between two buildings. Under practical conditions, the arrival angle of the laser beam changes slightly due to the mechanical vibration and atmospheric turbulence. Therefore, the communication devices are equipped with a beam tracking mechanism using 2-axis electromagnetic

mirrors. The system proposed in [22] achieves the throughput of 1.28 Tbps with WDM (32 × 40 Gbps). However, the tracking mechanisms of these systems do not support tracking and handover for high-speed trains.

Free-space optical communication for ground-to-satellite has also been proposed, specifically between a low earth orbit (200 to 1,000 km altitude) satellite and the ground. In ARTEMIS [23], the throughput of the downlink and the uplink is 1 Mbps and 50 Mbps, respectively. The National Institute of Information and Communications Technology (NICT) is planning to install HICALI (10 Gbps optical communication equipment) on a satellite to be launched in 2023 [24]. Additionally, free-space optical communication equipment is planned to be installed on SpaceX's next-generation Starlink [25]. Handover is not considered in these free-space optical communication system for ground-to-satellite, and tracking continues indefinitely once initiated.

Free-space optical communication has been also attracted great attention as a method of connecting servers in data centers [26]. A prototype system called FireFly [27] uses mirrors which are installed on the ceiling to change the direction of the communication light. However, the mirror angles are configured in advance and dynamic beam tracking is not really considered.

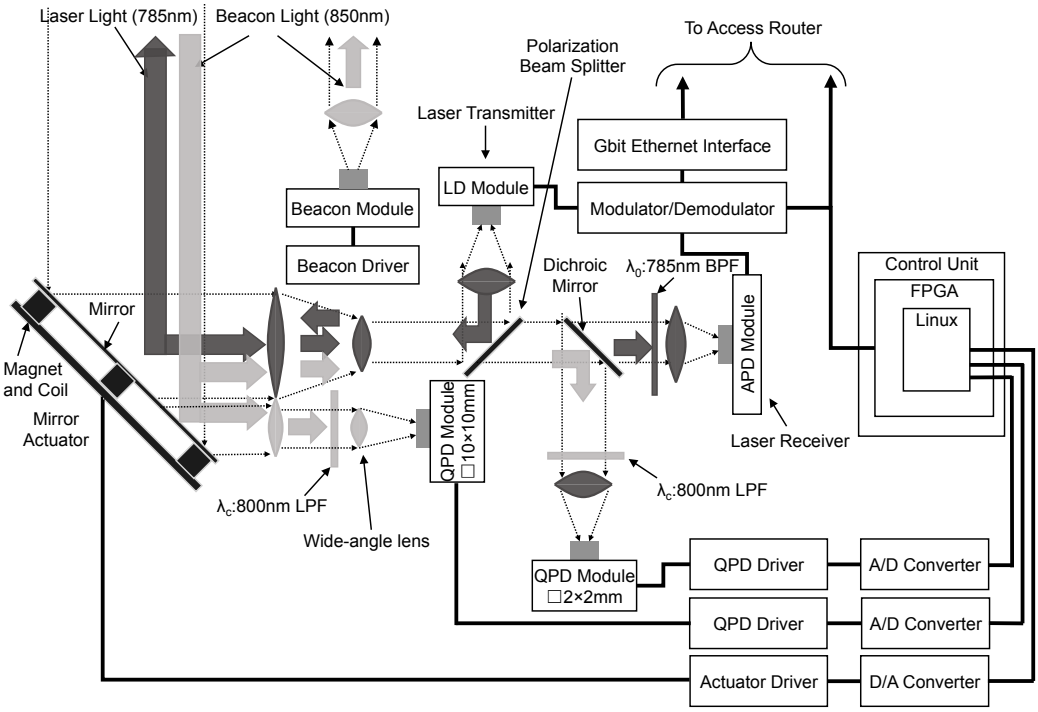

Figure 2.1: Block diagram of LTC12.

2.3 LaserTrainComm2012

2.3.1 Overview

Figure 2.1 shows a block diagram of LTC12 [10]. A LTC12 for a train is installed at the rear of the train while multiple LTC12s for the ground are installed along the railroad. LTC12 consists of a laser transmitter, a beacon transmitter, an optical receiver, an avalanche photo-diode (APD), a tracking mechanism, and a control unit on which Linux is running. Table 2.2 shows the specification of the control unit.

The laser light of 785 nm is used for communication. The laser trans-

Table 2.2: Specification of the control unit.

SZ410-U100	
CPU core	PowerPC405
CPU clock	350 MHz
Memory	32 MB * 2 (DDR2)
Flash memory	8 MB (SPI)
Operating system	Linux
Tracking frequency	1 kHz

mitter and the APD are designed to communicate at a 1 Gbps data rate when LTC12s are fixed at a stable location. A beacon module has infrared LEDs that send a beacon light signal to inform other LTC12 of its existence so that others can direct the laser beam to this LTC12. The infrared light of 850 nm is used for the beacon light signal.

2.3.2 Two-Dimensional Mirror Control

LTC12 has a tracking mechanism for directing the laser beam toward the beacon of the other side by using a control unit which controls the mirror's direction based on two quadrant photo-diode (QPD) modules, one with a wide-angle lens (*the wide-angle QPD*) and the other with a telescopic lens (*the telescopic QPD*). When the beacon light of a ground station is detected within the field of the view of the wide-angle QPD, the control unit directs the two-dimensional mirror actuator toward the ground station for initial acquisition. Once the optical link becomes stable, the control unit switches its input from the wide-angle QPD to the telescopic QPD for precise tracking.

2.3.3 Tracking and Handover Mechanism

Suppose that the mobile station is tracking the beacon light of a ground station. The mobile station is tracking the beacon light of the ground station accurately using the telescopic QPD. Since both the wide-angle QPD and the telescopic QPD are catching the beacon light of the ground station at the center of the sensors, the four voltage outputs of both QPDs are balanced, respectively (Fig. 2.2-(a)). Suppose that the train moves and the wide-angle QPD catches the beacon light of the next ground station. The four voltage outputs of the wide-angle QPD becomes unbalanced while those of the telescopic QPD remain balanced (Fig. 2.2-(b)). If the difference between the two horizontal (or vertical) voltage outputs of the wide-angle QPD exceeds the predetermined threshold, the mobile station starts the handover procedure. The mobile station begins to track the beacon light of the next ground station coarsely with the wide-angle QPD. Finally, the telescopic QPD catches the beacon light of the next ground station and the handover procedure finishes (Fig. 2.2-(c)).

2.3.4 Problems of LaserTrainComm2012

One of the problems of LTC12 is that it cannot precisely find the location of the beacon light signal, especially when there are several beacon lights because the QPD can only detect the direction of the beacon light. As a result, if there are multiple beacon light sources, the QPD detects the center

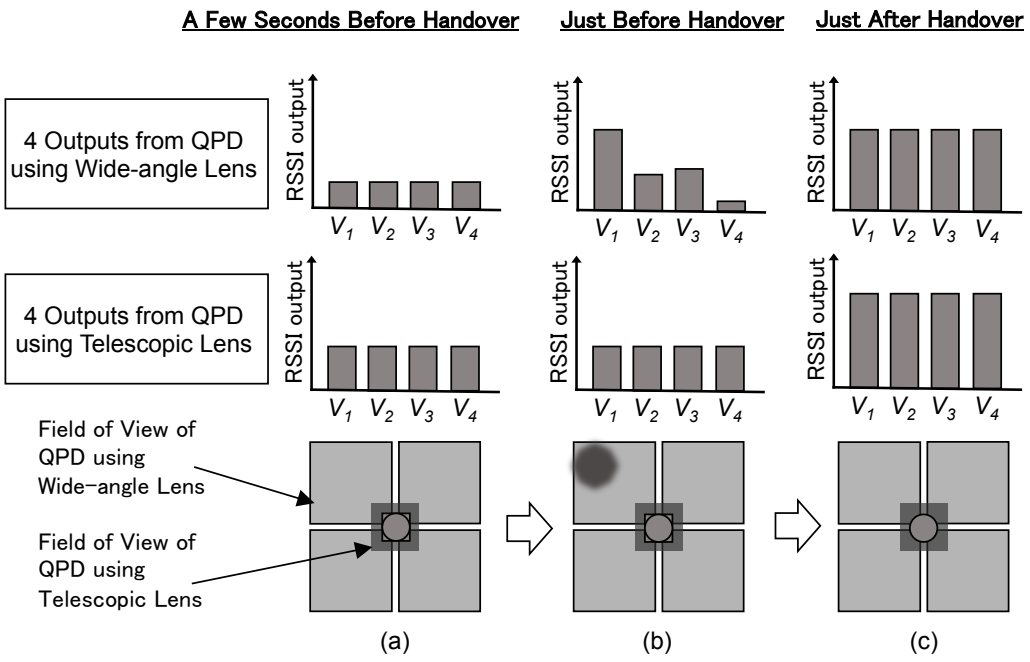

Figure 2.2: QPD output signals before and after handover.

of the power of the multiple beacon light sources but cannot differentiate among them. For example, in Fig. 2.2-(b), the wide-angle QPD detects the presence of intense light in the upper left direction, but it cannot detect the accurate distance between the current beacon position and the center of the QPD. LTC12 activates the mirror actuator at the tracking frequency (1 kHz) based on the QPD output, as shown in Table 2.2. The mobile station must repeat this process at a 1 ms interval to move the mirror slightly to the direction and check the output of the QPD. So the handover time of the LTC12 scheme is in the order of 40 ms in Layer-2.

Chapter 3

Rough Tracking by High-Speed Camera (LaserTrainComm2014)

3.1 System Design

Since LTC12 cannot precisely detect the location of the beacon light, it repeatedly moves the mirror little by little. LTC14 improves the handover performance compared with LTC12 with the use of a high-speed camera on a mobile station, which enables detecting the position of the beacon light of a ground station. Figure 3.1 shows a photo of LTC14.

3.1.1 Block Diagram

Figure 3.2 shows a block diagram of LTC14. Compared with the block diagram of LTC12, the wide-angle QPD is removed. Instead, the high-speed

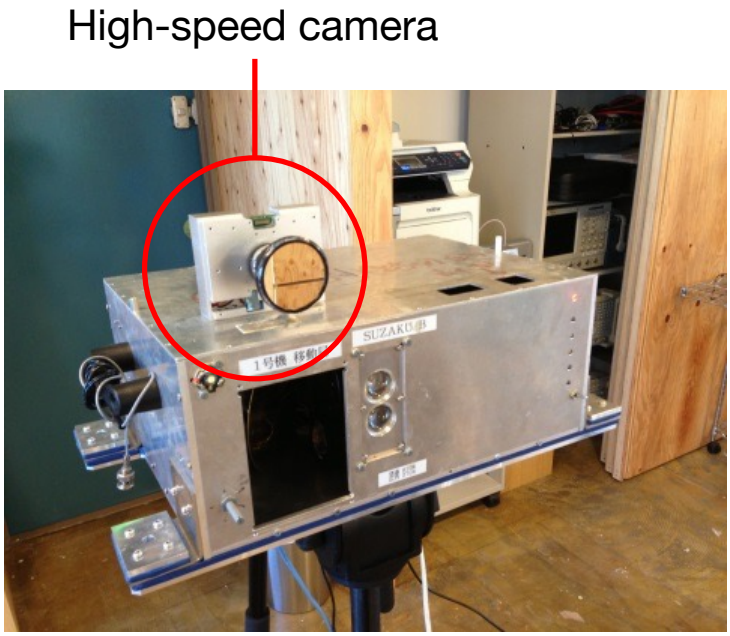

Figure 3.1: Photo of LaserTrainComm2014 (LTC14).

camera and the proximity sensor are added. Similar to LTC12, LTC14 consists of a laser transmitter, a beacon transmitter, an optical receiver, an avalanche photo-diode (APD), and a tracking mechanism. The laser transmitter and the APD are designed for communication at 1 Gbps data rate when transceivers are fixed at a stable location. The two-dimensional mirror actuator is controlled by the control unit which controls the mirror's direction based on data from the high-speed camera and the telescopic QPD.

3.1.2 High-Speed Camera

In order to achieve fast handover, the high-speed camera is used in LTC14 in order to detect an adjacent ground station to which a laser beam is handed

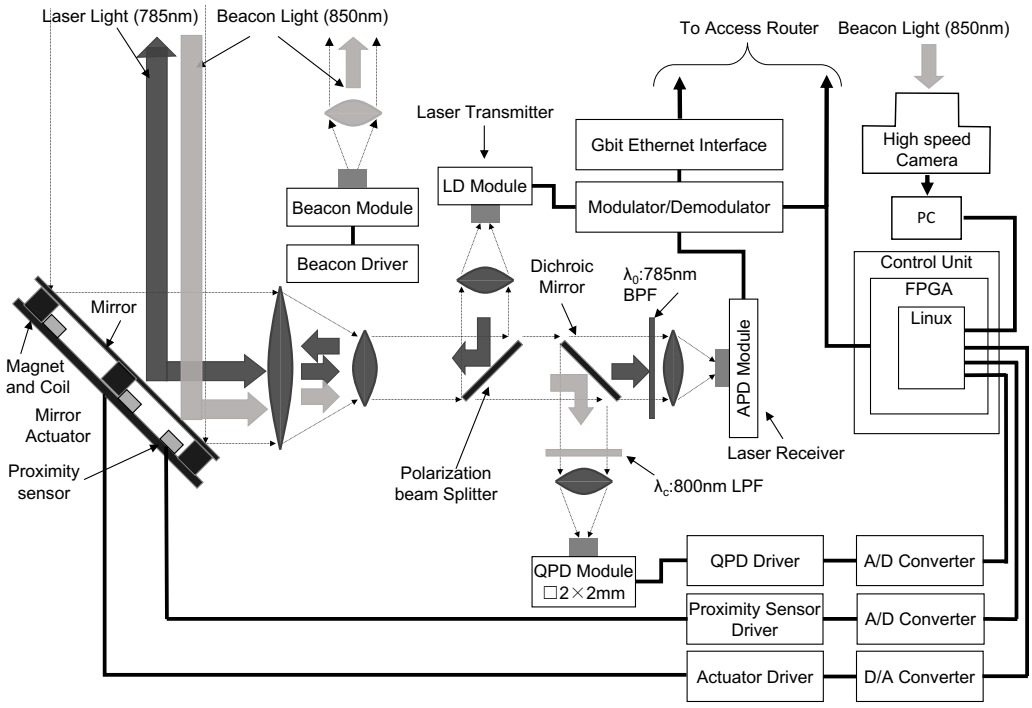

Figure 3.2: Block diagram of LTC14).

over. Fast beacon detection using the high-speed camera is developed to redirect the mirror quickly. The high-speed camera is able to detect 30 kHz square wave of the intensity modulation of the beacon light. Table 3.1 shows the specification of the high-speed camera.

3.1.3 Quadrant Photo Diode (QPD)

Once the laser beam is redirected to an adjacent ground station, the telescopic QPD is used for accurate tracking.

Table 3.1: Specifications of high-speed camera.

Product name	TOFCam Stanley P-300
Number of pixels	512 × 480
Size of pixels	30 μm × 30 μm
Chip Size	7 mm × 7 mm
Frame rate	20 fps
Output data	14 bits
Frequency of detectable beacon signal	30 kHz

3.1.4 Proximity Sensor

An Avago Technologies' HSDL-9100 infrared proximity sensor is used to detect the distance between the mirror and the base plate. The distance measured by this device is sampled every 1 ms, which was used for a feedback control of the mirror.

3.2 State Transition Diagram

Figure 3.3 shows the state transition diagram of the tracking algorithm in LTC14. The thick lines show the regular state transitions. When the power of the mobile station turns on, neither the high-speed camera nor the telescopic QPD detects beacon light (the *No beacons* state).

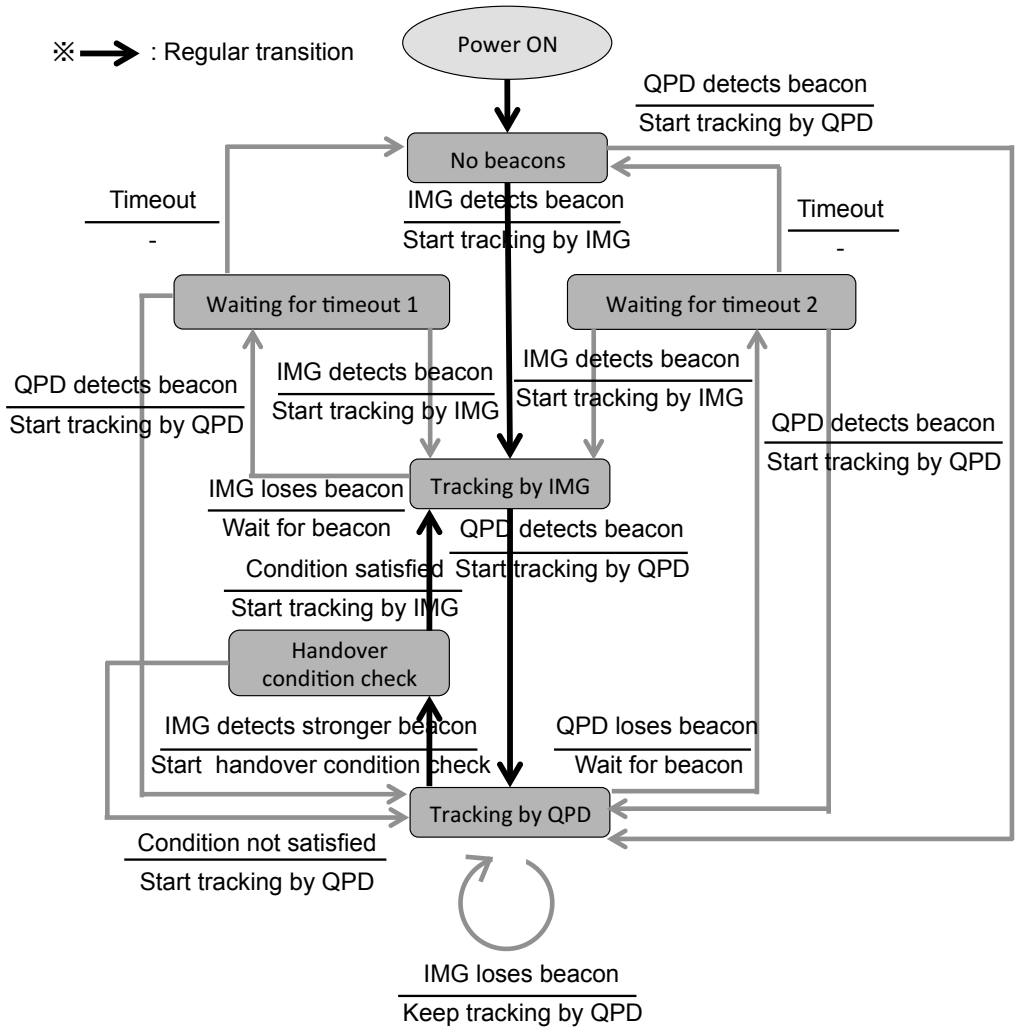

Figure 3.3: State transition diagram of LaserTrainComm2014 (LTC14).

3.2.1 Beacon Acquisition

Suppose that the high-speed camera of the mobile station finds the beacon light of a ground station. The mobile station starts tracking using the high-speed camera (the *Tracking by IMG* state). After tracking by the high-speed camera, the telescopic QPD also finds the beacon light of the ground station and the mobile station starts tracking using the telescopic QPD (the *Tracking by QPD* state). This state is the steady state in which both the mobile station and the ground station keep tacking each other.

3.2.2 Handover

Suppose that the beacon light of a new ground station appears in the view of the high-speed camera. The high-speed camera detects stronger beacon light and the mobile station starts the handover condition check procedure (the *Handover condition check* state). The mobile station does not start the handover procedure just after acquiring the beacon light of a new ground station by the high-speed camera. The mobile station starts the handover procedure after all the following conditions are satisfied:

1. the new beacon light image comes near the center of the view beyond the threshold and
2. the number of pixels of the new beacon light image is larger than that of the current beacon image.

The condition-(1) is introduced to make the handover time shorter. If the mobile station starts handover just after acquiring the beacon light of a new ground station, the angle of mirror movement for handover would be large. The condition-(2) is introduced to make sure that the new beacon light comes from the new ground station. If the handover conditions are satisfied, the mobile station starts tracking using the high-speed camera (the *Tracking by IMG* state). Just after that, the telescopic QPD also finds the beacon light and the mobile station returns to the steady state (the *Tracking by QPD*).

3.2.3 Temporal Shadowing

Figure 3.3 also takes into account accidental events, e.g., losing the beacon light by obstacles. If the telescopic QPD loses the beacon light in the steady state, the state changes to the *Waiting for timeout 2* state. If the beacon light is temporarily shadowed by obstacles such as a bird, the telescopic QPD would find the beacon light soon and the state returns to the steady state. If the shadowing time is long and the telescopic QPD does not catch the beacon light but the high-speed camera does, the state changes to the Tracking by IMG state.

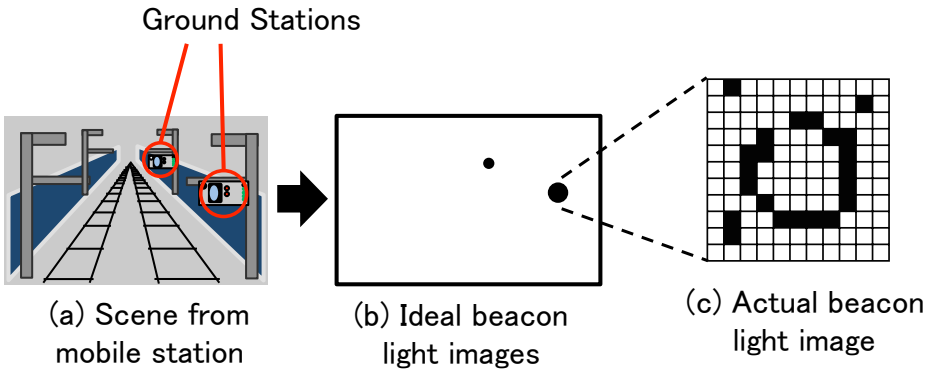

Figure 3.4: Beacon light images.

3.3 High-Speed Detection and Acquisition of Beacon Light Using Camera

In LTC14, the high-speed camera catches the beacon light and detects not only its power but also its position. Figure 3.4-(a) shows an example scene from the mobile station. In this example, two ground stations exist along a railway in the scene. If the output of the high-speed camera is ideal, only two beacon light images exist in the scene as shown in Fig. 3.4-(b), i.e., the positions of both beacon light images are detected and the beacon light of the closer ground station has a larger image. However, the actual image is not ideal as shown in Fig. 3.4-(c). Therefore, some image processing is necessary to correctly detect beacon light by the high-speed camera.

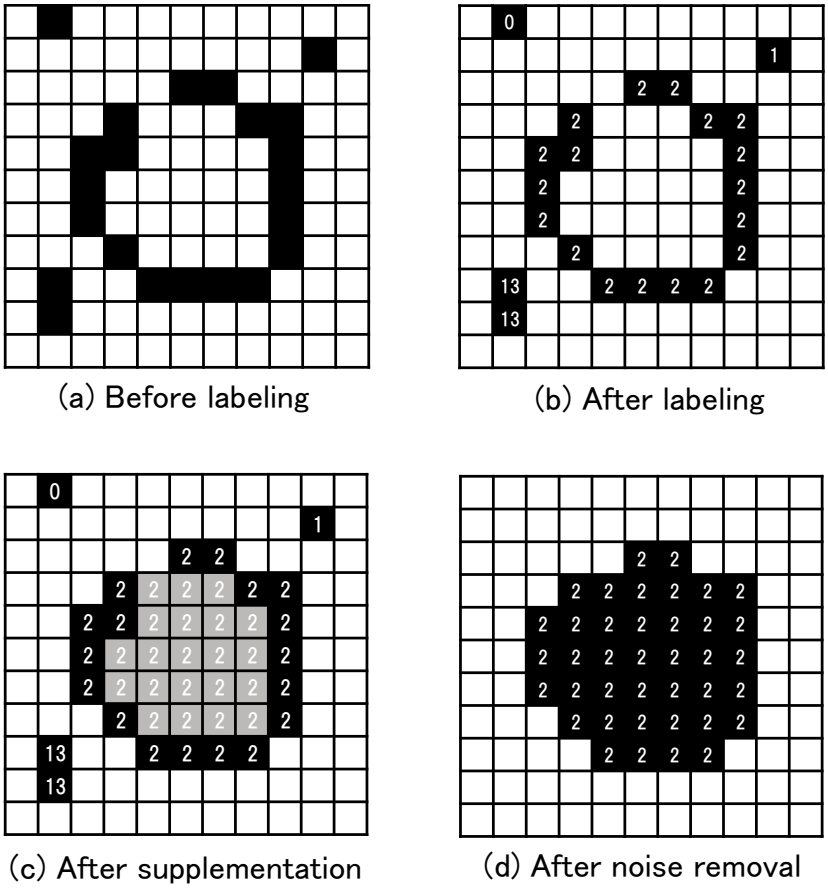

Figure 3.5: Image processing.

3.3.1 Recognition and Labeling of Beacon Light

First, for each pixel, the output value of the high-speed camera is transformed to a binary value based on a predetermined threshold. As a result, the image shown in Fig. 3.4-(c) is obtained. A black pixel means the value "1" while a white pixel means the value "0." As the figure shows, the center of the beacon light is not detected as "1" and the circumference of the beacon light image is broken in places. This is because the output value of the high-speed

camera is saturated due to too strong beacon light in the center. In addition, there are some noises.

Three kinds of image processing for supplementing a real image toward an ideal image are necessary: (1) labeling, (2) pixel supplementation, and (3) noise removal. The labeling procedure is as follows. The original image is shown in Fig. 3.5-(a). In this figure, the value of "0" is not shown. Focusing on a pixel, the eight neighboring pixels of the focused pixel are labeled with the same label as the focused pixel. As a result, the pixels that have the value "1" are assigned labels as shown in Fig. 3.5-(b).

The next step is pixel supplementation. The blank pixels that lie vertically or horizontally between the two pixels that have the same label are also labeled with the same label. As a result, the image shown in Fig. 3.5-(c) is obtained. In this figure, the gray pixels are supplemented. After pixel supplementation, the power of a beacon light can be expressed with the number of pixels. More pixels a beacon image is composed of, closer the source of the beacon light exists.

The final step is noise removal. In this dissertation, a beacon light image that has less than 3 pixels is eliminated as noise. In the example, the pixels labeled with "0," "1," and "13" are ignored as noises. As a result, the image shown in Fig. 3.5-(d) is obtained.

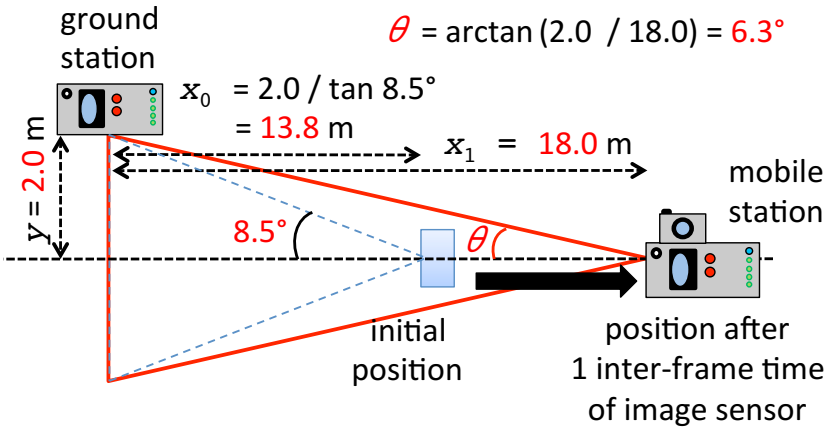

Figure 3.6: Relation between a ground station and a moving mobile station.

3.3.2 Inter-Frame Label Identification

The camera outputs a frame of a scene at the rate of 20 fps. Since the labeling procedure is performed in frame by frame independently, a label assigned to a beacon light image in a frame is different from a label assigned to the same beacon light image in the next frame. To keep tracking of the same beacon light, it is necessary to identify two beacon light images in two successive frames. It can be assumed that a beacon light image in a frame and that in the next frame are identical if the difference between their positions is less than a threshold because the maximum speed of a train is limited.

The threshold is calculated as follows. Figure 3.6 shows an ground station and a mobile station moving to right. Suppose that the mobile station finds the beacon light image of the ground station at the edge of the view of the high-speed camera at x_0 meters away from the ground station. Since the view angle of the high-speed camera used in LTC14 is approximately 17° and

the vertical distance (y) between the ground station and the mobile station in the figure is assumed to be approximately 2.0 meters, x_0 is calculated as $x_0 = 2.0/\tan 8.5^\circ = 13.8$ meters. Next, suppose that the mobile station moves to right at the speed of 300 km/h. After a single inter-frame time, i.e., 50 ms, the mobile station moves approximately 4.2 meters and the distance between the ground station and the mobile station becomes 18.0 meters (x_1). At this position of the mobile station, the angle θ is calculated as $\theta = \arctan 2.0/18.0 = 6.3^\circ$.

Next, let us calculate how many number of pixels the beacon light image moves after a single inter-frame time. As described above, at first, the beacon light image is located at the edge of the view and its angle is 8.5°. After a single inter-frame time, the beacon light image moves to the position where the angle is 6.3°. Since the half of the horizontal width of the view is 256 pixels, the number of pixels (P_m) that the beacon light image moves for a single inter-frame time is calculated as $P_m = 256 \times (1 - 6.3/8.5) \approx 66$ pixels. Thus, if the distance between two beacon light images in two successive frames is less than 66 pixels, it can be assumed that these two beacon light images are identical. P_m must be configured according to the speed of a train.

3.4 Evaluation

3.4.1 Evaluation Environment

Field experiments of LTC14 were conducted in a vehicle test course in February 21, 2014 to measure the performance and handover time using a car as shown in Fig. 3.7. The experiment setup is shown in Fig. 3.8. A mobile station was mounted on a car, and three ground stations were placed on the ground. The distance between a car and a ground station was 2 meters and the distance between adjacent ground stations were 100 meters. The car ran at the speeds of 30, 60, and 90 km/h. Using this setup, the behavior of the mirror at the time of beacon acquisition and tracking was measured as well as the handover time. Due to time limitation, only a few trials were conducted at each car speed.

3.4.2 Mirror Direction Measurement of Beacon Acquisition and Tracking

In Figs.3.9 to 3.11, the graph-(a) shows the horizontal mirror direction and the graph-(b) shows the tracking mode for 1 second before and after a handover at the car speeds of 30, 60, and 90 km/h, respectively. In the mirror direction graphs, the values of the Y-axis are the difference of the right and left proximity sensor's value and it can be assumed that these values are proportional to the mirror direction. The tracking mode graphs show which tracking mode (accurate, coarse, or no beacon) is used. In the accurate mode,

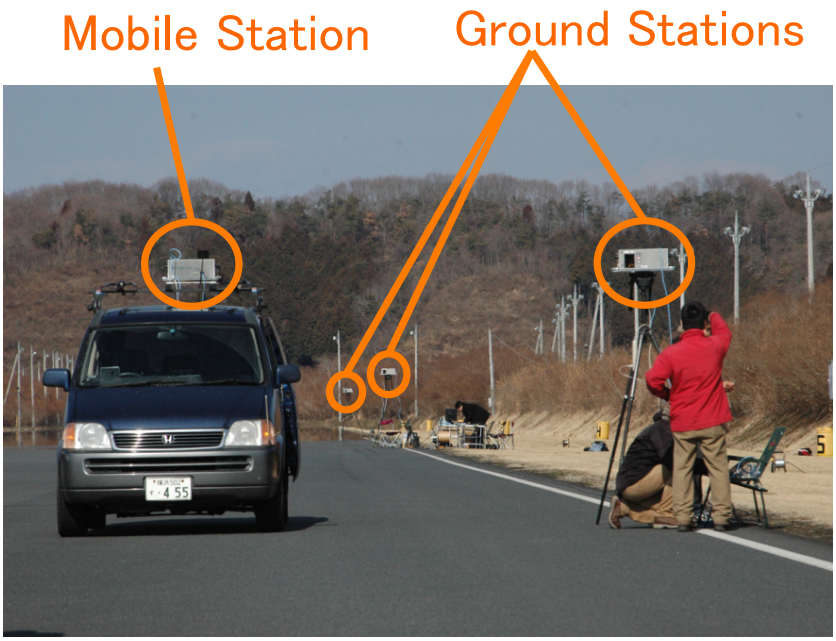

Figure 3.7: Handover experiments of LaserTrainComm2014 (LTC14) using a car.

the telescopic QPD is used while in the coarse mode, the high-speed camera is used.

At each car speed, the results show that at first, the tracking mode is the accurate mode and the mirror direction is almost stable. When the high-speed camera finds the beacon light of the next ground station, the tracking mode switches to the coarse mode and the mirror starts moving toward the next ground station. The tracking mode remains the coarse mode for approximately 80 ms, and then the tracking mode returns to the accurate mode when the telescopic QPD finds the beacon light of the next ground station. After that, the mirror continues to move toward the next ground

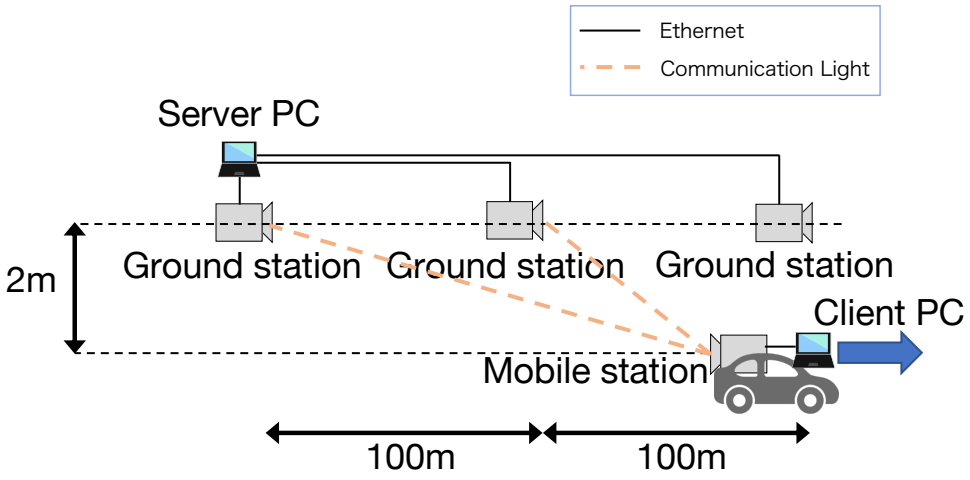

Figure 3.8: Experiment setup of LaserTrainComm2014 (LTC14).

station in the accurate mode. At the peak in the graph-(a), the handover procedure completes. Thus, the results show that the mirror of the mobile station was correctly directed toward the base station.

3.4.3 Disruption Time due to Handover

In Figs.3.9 to 3.11, the graph-(c) shows connectivity between the mobile station and one of the ground stations for 2 second before and after a handover at the car speeds of 30, 60, and 90 km/h, respectively. Note that the values of the X-axis in the connectivity graph are not synchronized with those of the mirror direction and tracking mode graphs because the machine used for connectivity measurement and the machine used for mirror direction and tracking mode measurement are different.

The connectivity was measured using the `ping` command, in which

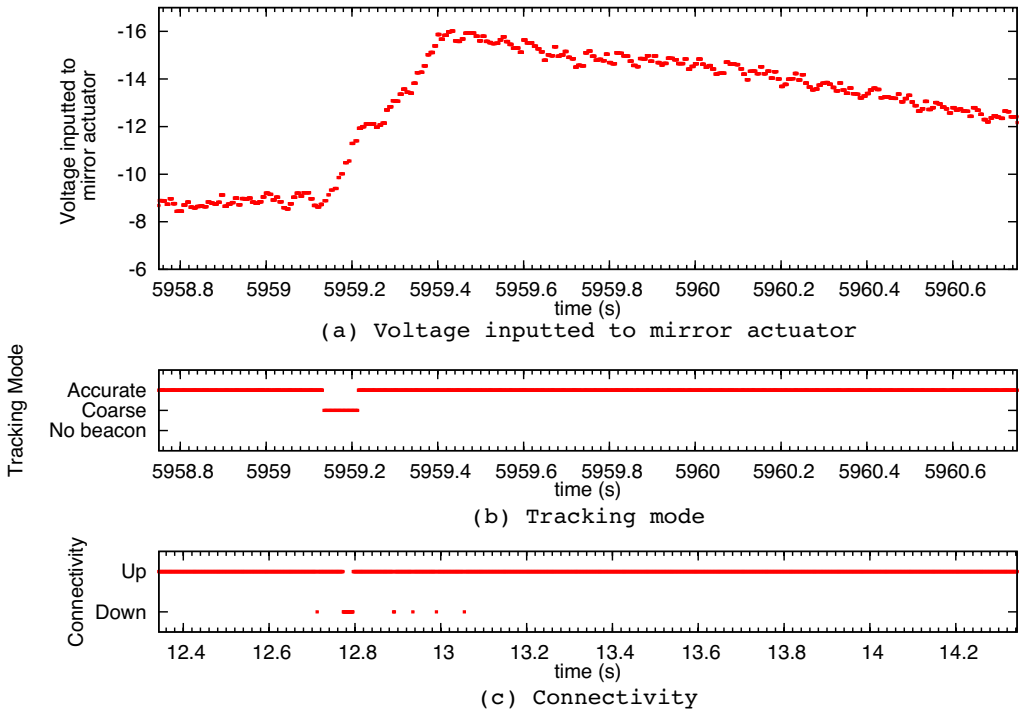

Figure 3.9: Mirror direction, tracking mode, and connectivity for 1 second before and after handover at 30 km/h.

an ICMP echo request packet is transmitted at a 1 ms interval. In the figure, "Up" means that a corresponding echo reply packet was received while "Down" means that a corresponding echo reply packet was not received. Table 3.2 summarizes the handover time against the car speeds.

The connectivity switches from the up mode to the down mode at approximately 45 ms after the tracking mode switches from the accurate mode to the coarse mode. The connectivity returns to the up mode even when the tracking mode remains the coarse mode. This is because the diameter of the laser beam of the ground station is so large that the optical receiver

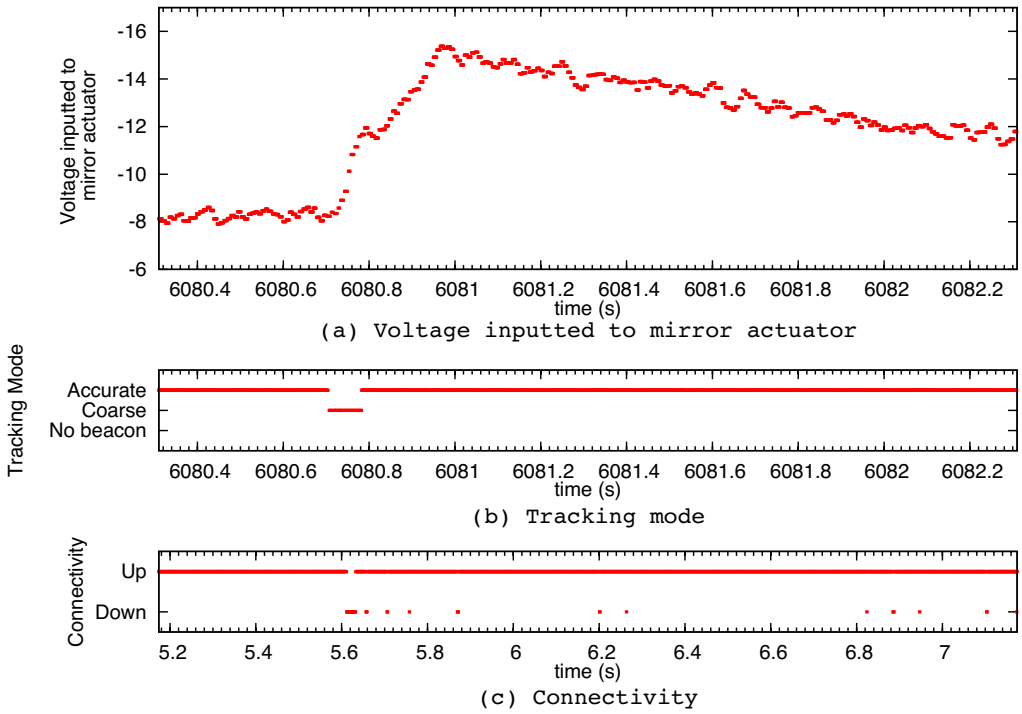

Figure 3.10: Mirror direction, tracking mode, and connectivity for 1 second before and after handover at 60 km/h.

of the mobile station can receive the laser beam of the ground station even when the handover procedure has not completed. The handover time at 60 km/h is shorter than that at 30 km/h. This is because the angle of mirror movement becomes smaller as the car speed becomes faster. In case of 90 km/h, just after handover, the telescopic QPD loses the beacon light, as shown in Fig. 3.11 (b) at 6390.78 sec and 6391.02 sec. Such behavior is not observed at 30 km/h and 60 km/h. One of differences among various speeds is the strength of vibration. Thus, I concluded that the telescopic QPD could not keep track of the beacon light due to large vibration and the narrow view

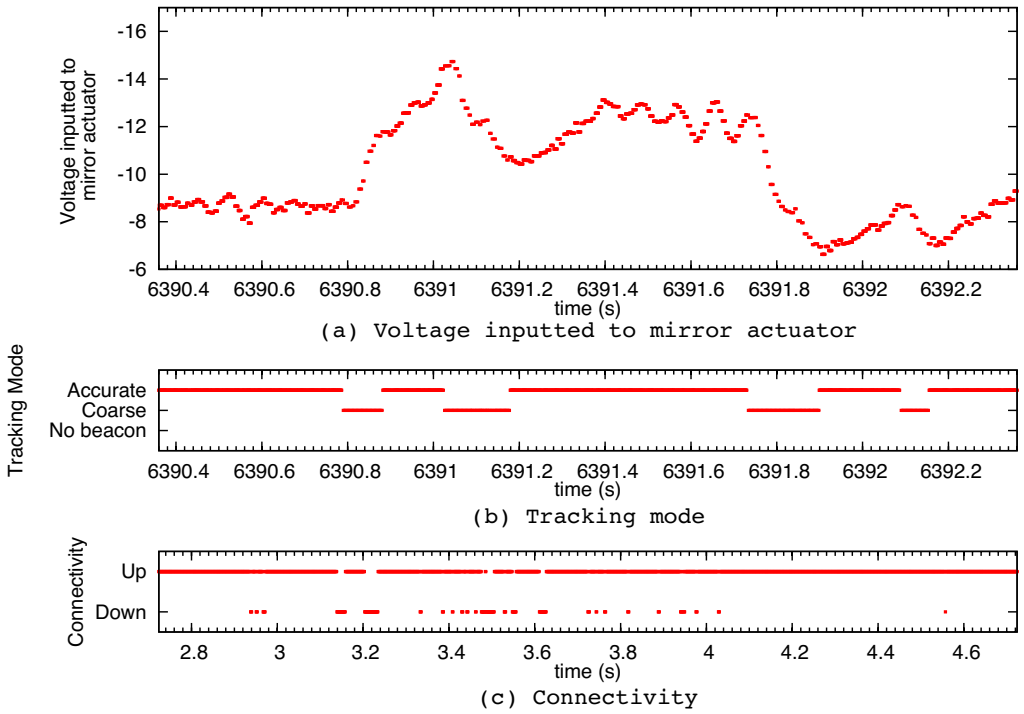

Figure 3.11: Mirror direction, tracking mode, and connectivity for 1 second before and after handover at 90 km/h.

angle of the telescopic QPD. To deploy LTC14 in in high-speed train such as Shinkansen, employing anti-vibration mechanisms would be required.

Table 3.2: Handover time in Layer-2.

	Car speed		
	30 km/h	60 km/h	90 km/h
Handover time	23 ms	21 ms	31 ms

3.5 Problems of LaserTrainComm2014

LTC14 tracks the communicating peer by changing the angle of the mirror with a two-axis actuator. Since the actuator was handmade, it is necessary to drive a single mirror with a single actuator and track the transmitted and received communication light and beacon light. As a result, the mirror had a diameter of about 10 cm, and the weight of the mirror increased accordingly. It is necessary to change the angle of the mirror largely at handover. As a result, it is found that the inertia at handover becomes large and the movement of the mirror overshoots. In addition, when the tracking mode switches from the coarse mode to the accurate mode, tracking becomes unstable due to errors of calibration between the coarse mode and the accurate mode. It took a long time for the mirror angle to stabilize during handover, resulting in a long communication disruption time. The angle of the mirror is adjusted on two axes by applying current to the electromagnets attached to the four corners on the back side of the mirror. In other words, the mirror actuator is driven by analog and open-loop control that changes the current flowing through the coil of the electromagnet. LTC14 cannot accurately detect the direction of the mirror controlled by changing the current. Finally, LTC14 identifies the beacon light only by the area on the image, so it may misidentify the reflected light of its own beacon light or sunlight as the beacon light of a communication peer.

Chapter 4

Improved Tracking and Handover Accuracy with Station ID (LaserTrainComm2022)

4.1 System Design

As mentioned in Sec. 3.5, LTC14 has the following problems:

1. instability just after handover due to the inertia of the large mirror, which causes overshooting at handover,
2. inaccuracy of the mirror actuator due to analog and open-loop control, which reduces communication quality, and
3. inability to identify each ground / mobile station, which causes misidentification of communication peer.

In order to solve these problems, LaserTrainComm2022 (LTC22) was developed. LTC22 employs two small mirrors for transmission and reception, respectively, to solve the problem (1). Digitally controlled mirror actuators are adopted to solve the problem (2). The station ID is encoded in the beacon light to solve the problem (3).

4.1.1 Block Diagram

Figure 4.1 shows a block diagram of LTC22. LTC22 uses LED beacons to notify the communication peer of the location of its own station. As described in Sec. 4.2, the station ID uniquely assigned to each LTC22 device is intensity-modulated and encoded in the beacon light. The dual-port camera of the communication peer captures the beacon light in which the station ID is encoded , i.e., the mobile station captures the beacon light from the ground station and the ground station captures the beacon light from the mobile station. The obtained image is sent to the system controller (Linux). Based on the information, the system controller drives the mirror actuators and changes the direction of the mirrors to track the communication light. On the other hand, communication light is transmitted and received by the optical communication device. In addition, in order to know the Up/Down status of the optical communication link between LTC22 devices, the amount of the received communication light is notified to the system controller. This makes it possible to monitor the optical communication link status.

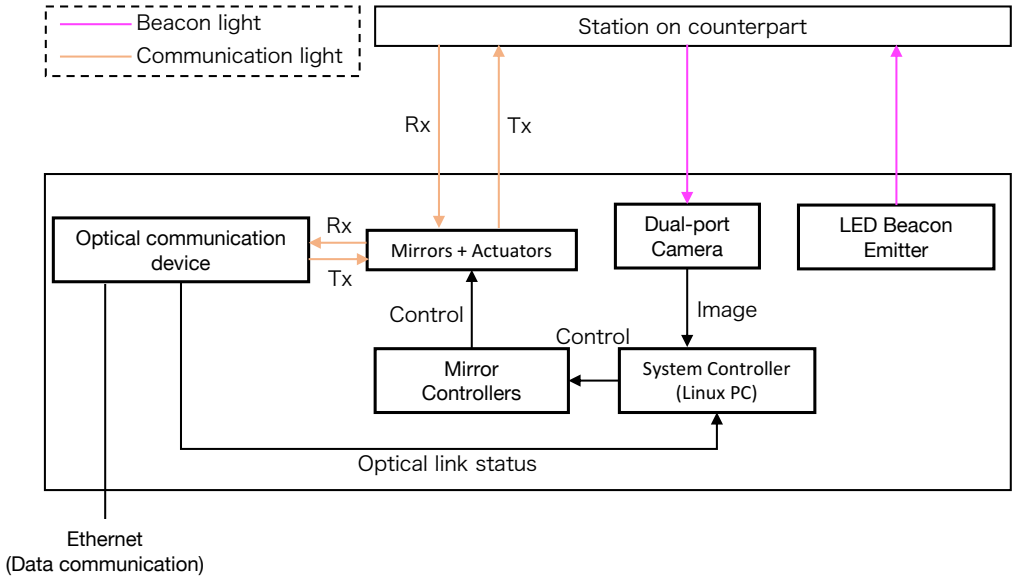

Figure 4.1: LaserTrainComm2022 (LTC22) block diagram.

4.1.2 Dual-Port Camera

Table 4.1 shows the specifications of the dual-port camera, which is a trial product. The product name is A5ZHP84 made by Hamamatsu Photonics K.K. The specification of the lens on the dual-port camera is shown in Table 4.2. The dual-port camera captures two types of images, a wide view image (with low fps) and a narrow view image (with high fps). The wide view and narrow view can be acquired independently. The wide view covers the entire pixels the dual-port camera has (656x248 pixels) while the narrow view covers part of the entire pixels such as 32x15 pixels as shown in Fig. 4.2. The position of the narrow view can be changed with a time overhead of 6 ms. Both intensity depths of the wide view and the narrow view are the same, 0 to 4,095 (without unit). If the strength of the beacon light is too high (e.g.,

Table 4.1: Specifications of dual-port camera.

	Pixel	**Viewing angle (Horizontal × Vertical)**	**Frame rate**	**Intensity depth**
Wide view	656 × 248	30 × 11 degrees	100 fps	0 to 4,095
Narrow view	32 × 15	1.5 × 0.7 degrees	8,000 fps	(without unit)

Table 4.2: Specifications of Lens.

Product name	LM12JC10M (Kowa Optronics Co.,Ltd.)
Focal length	12 mm

if a mobile station and a ground station are very close to each other), the intensities in the wide and narrow view images may exceed 4,095 and are saturated.

The lens of the dual-port camera is equipped with a filter to remove noise by cutting light with frequencies other than the beacon light. However, the filter has no effect on the reflected beacon light of the own station. In addition, since the sunlight contains the light with the same frequency as the beacon light, it is difficult to remove the noise only with the filter. To correctly identify the beacon light, the station ID is encoded in the beacon light as described in Sec. 4.2.

4.1.3 LED Beacon

Table 4.3 shows the specifications of the LED beacon. 100 LED emitters with lenses that emit infrared light are arranged on the front of LTC22 as an a array of 10 × 10. By adjusting the number of LED light emitters that are

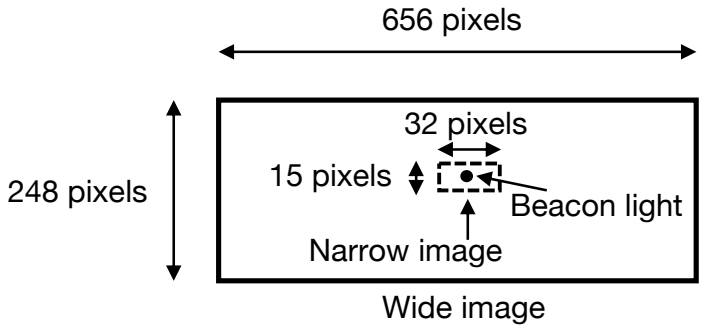

Figure 4.2: Wide view and narrow view.

Table 4.3: Specifications of LED beacons.

Wavelength	**Beam angle**	**Number of arrays**	**Blinking rate**
950 nm	20–30 degrees	10×10	Up to 10 MHz

on, the reach of the beacon light can be controlled. The amount of beacon light is not adjustable; only two patterns are possible: OFF (0 %) and ON (100 %). A microcomputer, ESP32-WROOM-32, is connected to the LED beacon, which controls the blinking of the LED light emitters. The blinking rate of the LED beacon is up to 10 MHz according to the specification. In practice, the blinking rate is configured as 2.5 MHz (400 ns cycle) because the LED beacon is not correctly blinking if the blinking rate is configured to higher than 2.5 MHz. As described in Sec. 4.2, the station ID is encoded in the beacon light with a blinking pattern. Since it is assumed that the station ID remains unchanged in actual operation, the same blinking pattern is periodically repeated in each LTC22 device.

Table 4.4: Specifications of mirror actuators.

	Horizontal	**Vertical**
Model	Canon GM-1015	Thorlabs DDR100/M
Scanning angle	20 degree	360 degree
Setting time	390 µs	200 ms

4.1.4 Mirrors and Mirror Actuators

LTC22 has two separate mirrors for transmitting light and receiving light, respectively. The size of the mirror is approximately 3 cm × 4 cm, which is much smaller than that in LTC14. The small size mirrors avoid the mirror drive overshooting occurred in the LTC14 at handover.

LTC22 has independent actuators for horizontal and vertical rotation of the mirrors. As shown in Fig. 4.3, there are two horizontal actuators for the transmission light and the reception light respectively, and there is a single vertical actuator on which the two horizontal actuators are installed. Table 4.4 shows the specification of the actuators. As shown in Table 4.4, the setting time of the vertical actuator is too slow to track the communication peer when vertical vibration occurs. Since the two horizontal actuators are mounted on a stand which is rotated by the vertical actuator, a high torque is required for the vertical actuator. The vertical actuator used in LTC22 was the best choice among actuators that satisfy the required torque.

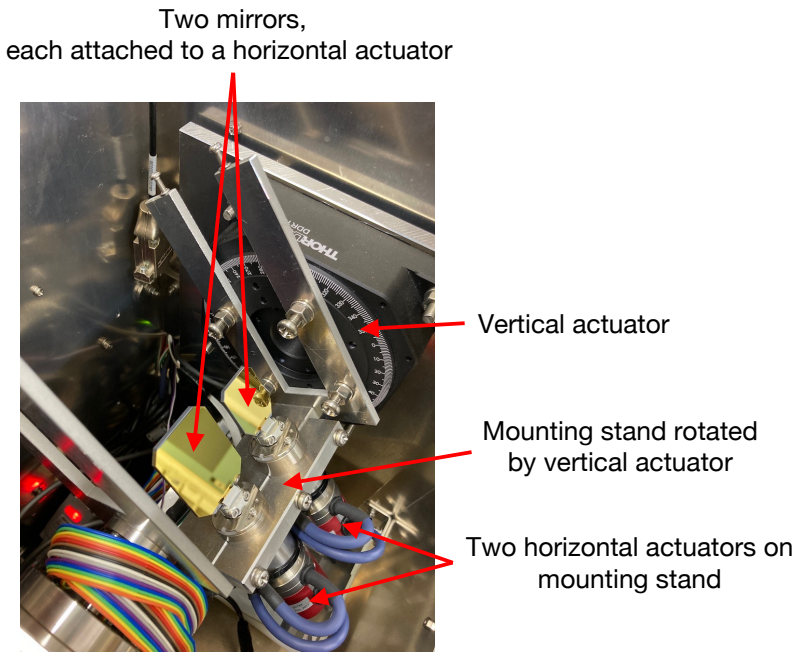

Figure 4.3: Appearance of mirror actuators in LTC22

4.1.5 System Controller

The LTC22 uses Analog Devices ADRV9361-Z7035 equipped with Xilinx's Zynq-7000 as the system controller, on which Linux is running to control the entire system. A part of the memory on the board is used as a DMA buffer, to which the image from the dual-port camera is written. Figure 4.4 shows the structure of the buffer for transferring images from the dual-port camera to Linux. The two buffers are prepared for wide view and narrow view, respectively. Each buffer is composed of several frame blocks, to each of which a captured image is stored. A frame block is composed of the block number field, the image position field, and the intensity fields, each of which

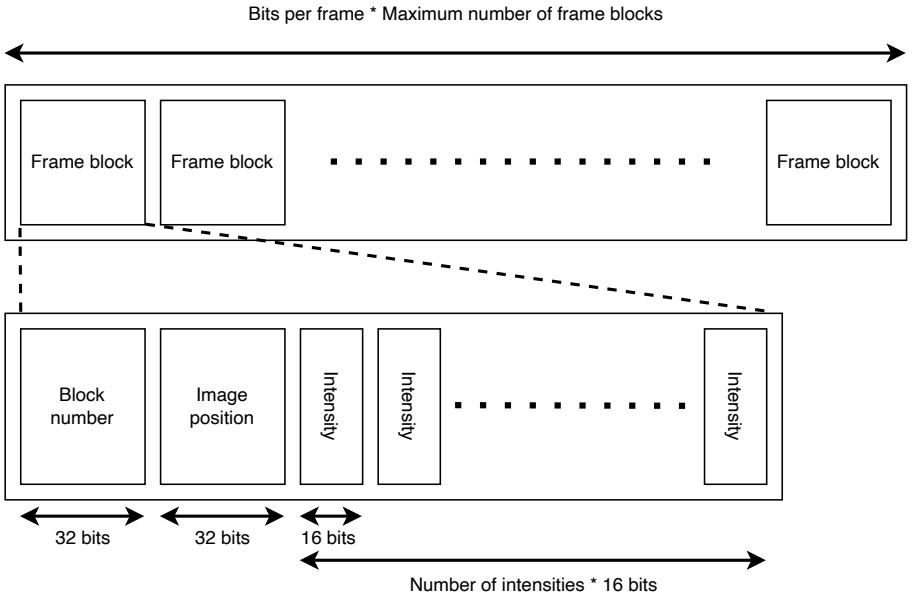

Figure 4.4: Buffer for image transfer (Upper: Buffer. Lower: Detail of a frame block).

indicates the brightness of the corresponding pixel. The maximum number of the block frames in each buffer is 2 for the wide view buffer and 256 for the narrow view buffer. The dual-port camera continuously writes a captured image to a frame block in a ring buffer manner for the wide view and narrow view images, respectively.

The system controller can get the block number, the image position, and the pixel brightness for each frame block. Block numbers are assigned to frame blocks in chronological order, and are used to determine which frame block is currently being written in the buffer. For example, assume that the number of frame blocks is five and block numbers are "2", "$2^{32}-1$", "2^{31}", "0" and "1" in Fig. 4.4. Then a block number which is currently being

written in the buffer is "2". The image positions indicate the lower right corner of the image in the entire camera image. The image positions of the wide view always (0, 0) while the image positions of the narrow view indicate the positions of the lower right corner of the image.

4.1.6 System Configuration

Figure 4.5 shows the system details, and Figs. 4.6 and 4.7 show the appearance of the actual system. Originally, it was planned that a product of 10 Gbps optical communication device is equipped with LTC22, which has been developed since 2017 by Toyo Electric Corporation. Because it was not commercialized in time, SOT-US100, a product of 100 Mbps infrared communication device made by Toyo Electric Corporation is equipped with LTC22 instead. Table 4.5 shows the specification of SOT-US100.

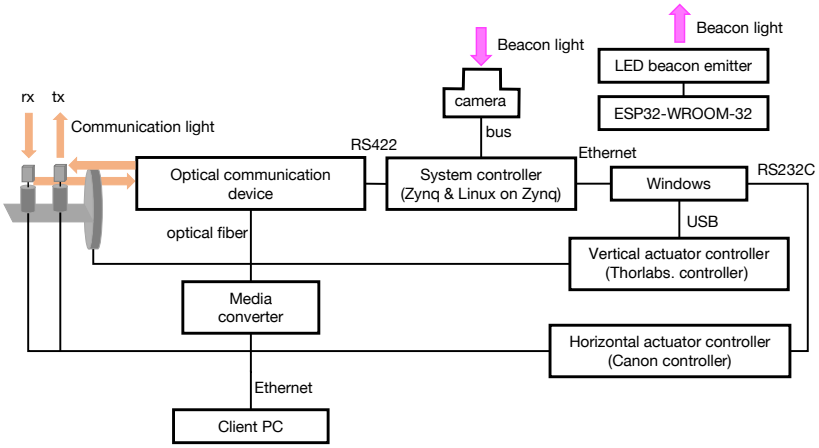

Figure 4.5: System Details.

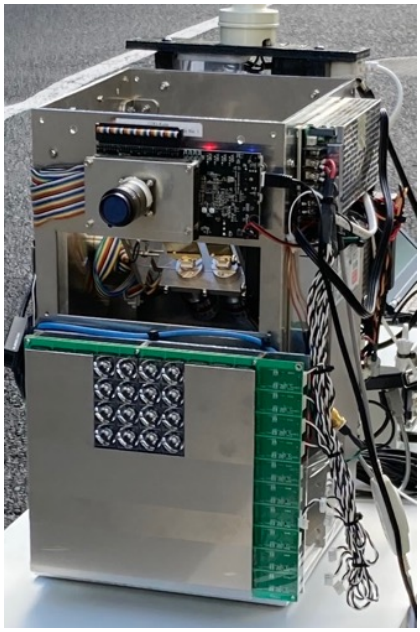

Figure 4.6: System appearance 1.

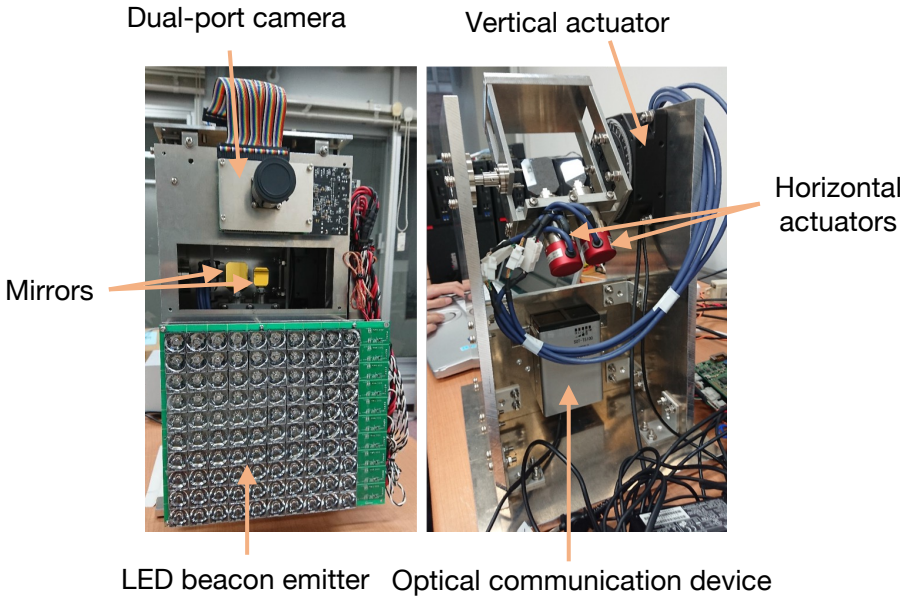

Figure 4.7: System appearance 2.

Table 4.5: Specifications of optical communication device.

Product name	SOT-US100 (Toyo Electric Corporation)
Beam angle	1.2 degree
Link rate	100 Mbps
Wavelength	860 mm

Since the drivers for the horizontal and vertical mirror actuators used in LTC22 are provided only for Windows, a separate Windows PC is required in addition to the system controller. Therefore, commands from the system controller are sent to the mirror actuators via the Windows PC. In order to drive the mirror actuators, the system controller sends the beacon light positions in the image to the Windows PC. In the Windows PC, two processes for the horizontal and vertical actuators are running, and they receive the beacon light positions. Based on the pre-calibrated information, each process converts the beacon coordinates to the angle of the mirror(s), and drives the mirror actuator(s).

4.2 Coding and Modulation of Station ID

4.2.1 Station ID Coding

In LTC22, a station ID is modulated by intensity modulation using 2 PPM (2 Pulse Position Modulation). The modulation method is shown in Fig. 4.8. The length of a slot is 1/4,000 second (0.25 ms) and each slot takes either HIGH or LOW state. Since the frame rate of the narrow view is approximately 8,000 fps, a slot is sampled with two successive narrow view images on

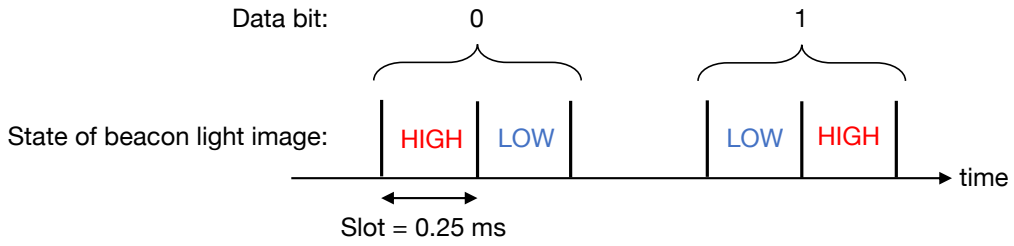

Figure 4.8: Station ID coding.

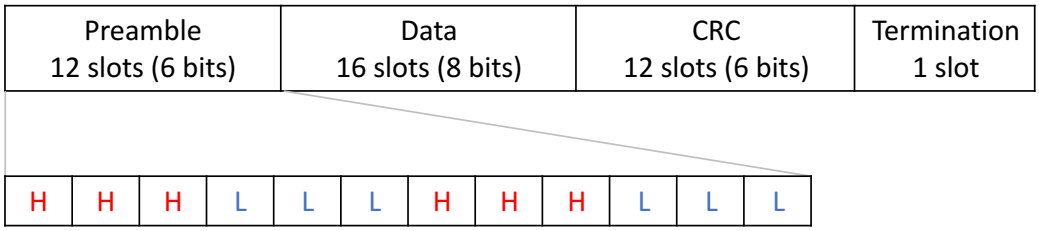

Figure 4.9: Station ID frame.

average. For 1-bit data, "HIGH + LOW" represents 0 and "LOW + HIGH" represents 1.

The station ID frame structure is shown in Fig. 4.9. A station ID frame consists of a preamble part, a data part, a CRC part, and a termination part.

The preamble part indicates the beginning of the station ID frame and is a special 12-slot pattern that does not appear in other parts. The preamble part is also used for clock synchronization between the beacon sender and the beacon receiver. In the data part, the station ID is stored in 16 slots (8 bits) in accordance with the 2PPM modulation method described above. The CRC (Cyclic Redundancy Check) part is a 12-slot pattern used to detect errors in the data part. The termination part is a one-slot pattern that is

always LOW to distinguish it from HIGH at the beginning of the preamble part.

Since the station ID frame consists of 41 slots, approximately 82 narrow view images (about 10.25 ms) are required to transmit a station ID frame. In practice, the timing of the blinking rate of the beacon light and the frame rate of the narrow view image are not synchronized. Therefore, twice the time for transmitting a single station ID frame (approximately 20.5 ms) is required for a single station ID frame. As discussed in Section 4.3, the process for station ID demodulation is done before the handover decision and does not affect the handover time.

4.2.2 Station ID Modulation

As described in Sec. 4.1.3, the amount of light is not adjustable; only two patterns are possible: OFF (0 %) and ON (100 %). In the wide view, the two states (HIGH and LOW) must change according to the frame rate (approximately 100 fps; 10 ms) because the difference image of two successive images is used to detect beacon candidates as described in Sec. 4.2.3. At the same time, in the narrow view, the two states (HIGH and LOW) must change according to the frame rate (approximately 8,000 fps; 0.125 ms) to demodulate the station ID. Since the two successive narrow view images are used for sampling a slot to improve the accuracy of deciding the state of the slot (HIGH or LOW), the slot length is set to 0.25 (0.125×2) ms In summary, the LED must be blinking so that the wide view recognizes the

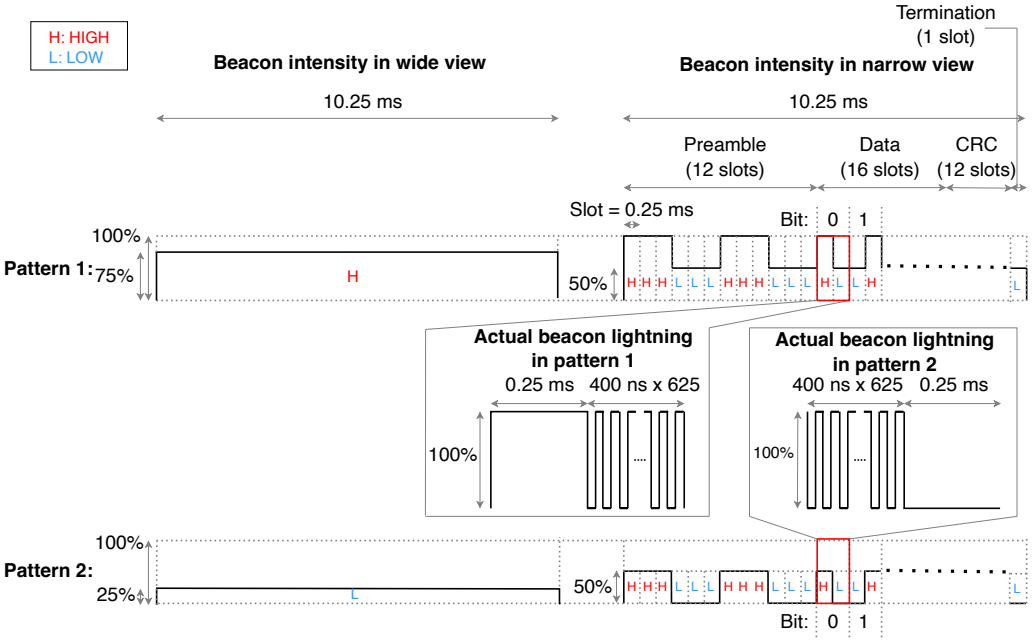

Figure 4.10: Actual beacon lighting (two patterns).

HIGH or LOW state at a 10 ms interval and the narrow view recognizes the HIGH or LOW state at a 0.25 ms interval at the same time.

In order to enable this, two patterns of LED blinking are introduced as shown in Fig. 4.10. In the pattern 1, the LED is continuously ON throughout a slot and it is blinking ON and OFF at a 400 ns interval throughout a slot. In the pattern 2, the LED is continuously OFF throughout a slot and it is blinking ON and OFF at a 400 ns interval throughout a slot. In the pattern 1, the narrow view recognizes the continuously ON slot as 100 % beacon light intensity. In the pattern 2, the narrow view recognizes the continuously OFF slot as 0 % beacon light intensity. In both patterns, the narrow view recognizes the blinking slot as 50 % beacon light intensity.

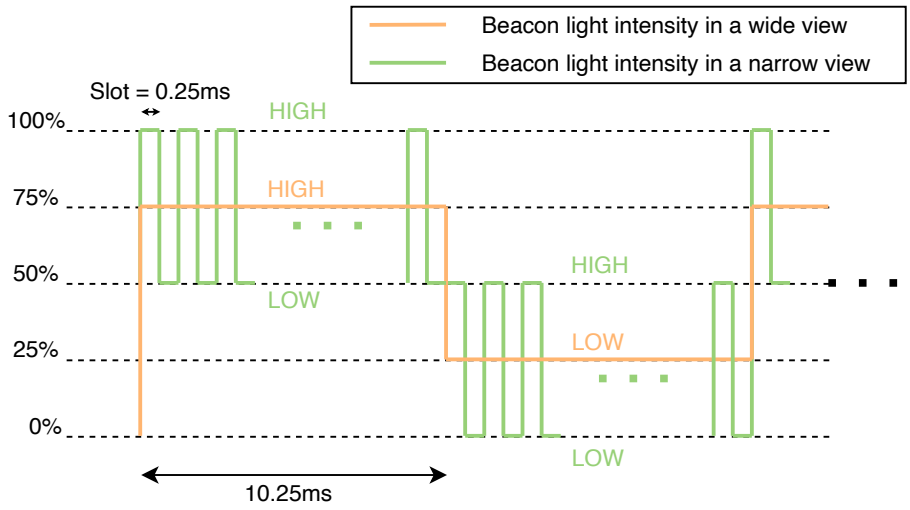

Figure 4.11: Beacon light intensity in the wide view image and the narrow view image.

On the other hand, if the pattern 1 continues throughout the interval of the wide view, the wide view recognizes 75 % beacon light intensity, which can be defined as the HIGH state. If the pattern 2 continues throughout the interval of the wide view, the wide view recognizes 25 % beacon light intensity, which can be defined as the LOW state. In the narrow view, if the wide view is the HIGH state, the narrow view recognizes 100 % beacon light intensity as the HIGH state while 50 % beacon light intensity as the LOW state. If the wide view is the LOW state, the narrow view recognizes 50 % beacon light intensity as the HIGH state while 0 % beacon light intensity as the LOW state. The beacon lighting in the wide view and the narrow view is shown in Fig. 4.11.

4.2.3 Beacon Capturing

Figure 4.12 shows the beacon detection method in the wide view. A wide view image may contain noise such as sunlight which cannot be distinguished from the beacon light. In order to remove noise in the wide view image, the difference image of two successive wide view image is used. Since the beacon light intensity changes at the frame rate of the wide view, noise such as sunlight disappears in the difference image of two successive wide view images. In the difference image, the intensity of the beacon light image remains strong while the intensity of noise greatly reduces.

In practice, the beacon light image is composed of multiple pixels, whose size depends on the brightness. After the difference image is generated, each pixel is binarized based on its intensity and the threshold value for labeling. This threshold value for labeling is determined through experiments in an outdoor environment. The areas composed of the pixels binarized as "1" are labeled using a labeling algorithm. Each labeled area is a beacon candidate. In LTC22, the labeled composed of the maximum number of pixels is assumed to be a beacon light candidate.

After a beacon light candidate is decided, a station ID is demodulated using the narrow view images and the position of the beacon candidate as follows. First, the position of the narrow view is moved so that the beacon candidate is captured at the center of the image. Then, the narrow view images are stored in the narrow view buffer in chronological order. Since the

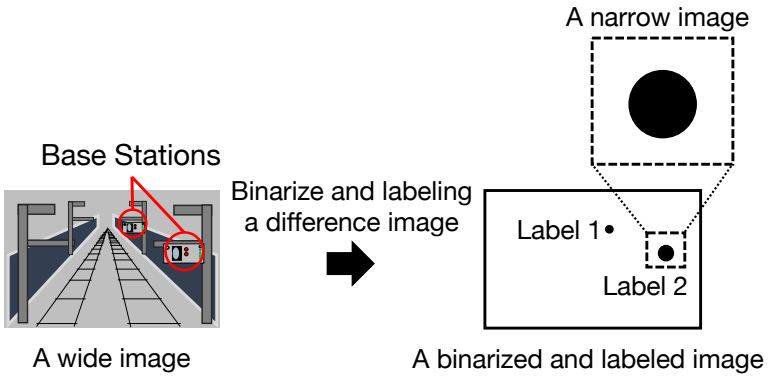

Figure 4.12: Beacon detection in a wide view.

beacon light receiver is not synchronized with the beacon light sender, the narrow view images containing two station IDs (165 images, approximately 20.5 ms), which contain at least one station ID frame, are used to demodulate a station ID.

In the narrow view, the center of the beacon light candidate is calculated again to accurately decide the state (HIGH or LOW) of the slots that compose a station ID frame as follows. A difference image is generated from the first and second narrow view images in the narrow view buffer. The difference image is binarized and labeled using the labeling algorithm in the same manner in the wide view. If the labeled area with the largest size is smaller than the threshold value for labeled areas (e.g., 3 pixels), the next difference image generated from the second and third ones is used. This step is repeated until a labeled area that has the size larger than the threshold value for labeled areas is found. The process is usually completed after two or three iterations although 164 difference images may be generated from 165

images.

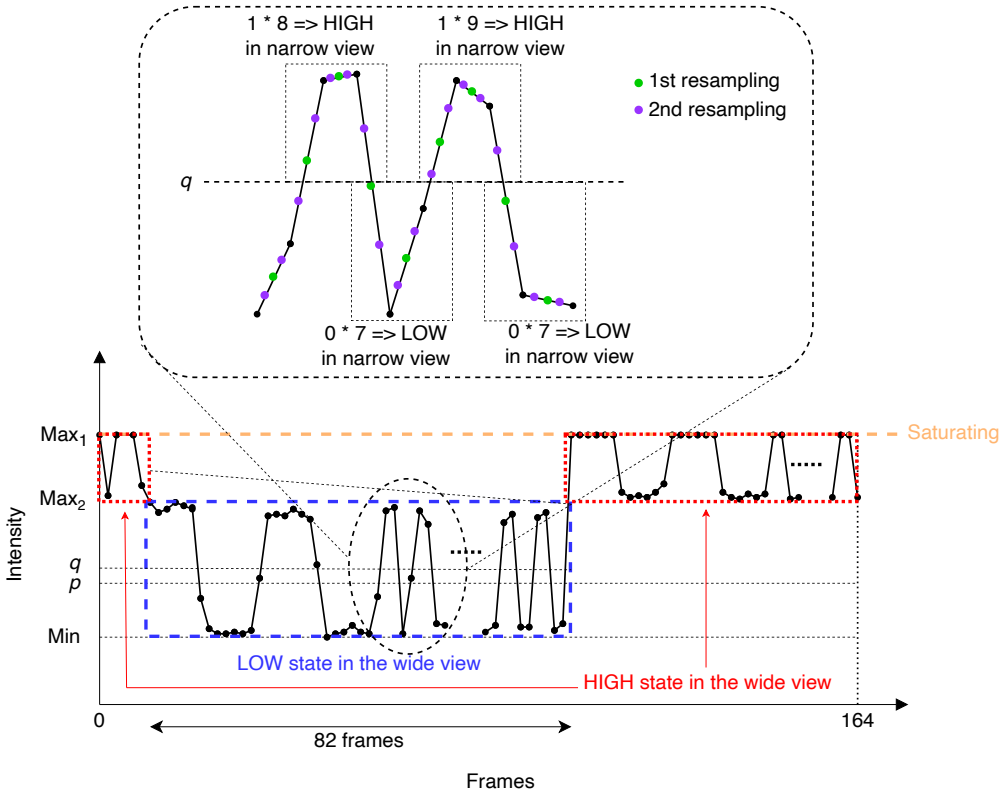

Figure 4.13: Frame-by-frame variation of the center of the beacon candidate's intensity.

Once the center of the beacon light candidate is determined successfully, the intensity of the center of the beacon light candidate is obtained as the average of the intensities in the 164 difference images. Figure 4.13 shows an example of frame-by-frame variation of the center of the beacon light candidate's intensity. The frames in the HIGH state in the wide view may be saturated, especially when a mobile station and a ground station are very close to each other. Therefore, the frames in the LOW state in the wide view

are used for demodulation of a station ID in the narrow view. The threshold value p for deciding the state in the wide view is obtained from formula (4.1) to identify whether the wide view is the HIGH state or the LOW state as shown in Fig. 4.11. Fig. 4.13 also shows the threshold p.

$$p = Min + (Max_1 - Min) * 0.25 \tag{4.1}$$

The interval in which 82 frames (required to demodulate a single station ID) whose intensity is below the threshold value p do not appear consecutively is defined as "the HIGH state in the wide view" in Fig. 4.11. Another interval is defined as "the LOW state in the wide view."

Once the "the LOW state in the wide view" is found, the intensities are re-sampled twice using an average of the intensities of the successive two frames as shown in Fig. 4.13. The number of the intensities becomes four times the original number of the intensities. As a result, the variation of the intensities (the lower figure in Fig. 4.13) is smoothed (the upper figure in Fig. 4.13).

The threshold value q for binarization is obtained from formula (4.2) to binarize the intensities in the 82 frames in "the LOW state in the wide view."

$$q = Min + (Max_2 - Min) * 0.5 \tag{4.2}$$

The station ID is demodulated from the binarized values. Since a slot in the station ID is sampled by successive 8 intensities (2×4 by resamplings), a binary value of "00000000" (eight consecutive "0"s) indicates the LOW state in the narrow view, and a binary value of "11111111" (eight consecutive "1"s) indicates the HIGH state in the narrow view.

However, the blinking rate of the beacon light is not synchronized with the frame rate of the narrow view image. Noise may appear in the binarized values. Considering noise in the binarized values, up to plus or minus two of the reference number of consecutive "0" or "1" is acceptable, i.e., six to ten consecutive "0" or "1" are acceptable. Table 4.6 shows the rules for how to interpret binarized values as HIGH slot(s) or LOW slot(s). If sequences of binarized values not listed in Table 4.6 are detected, the demodulation of a station ID is assumed to be failed.

Table 4.6: Rules for how to interpret binazied values to HIGH slot(s) or LOW slot(s).

		Value	
		0	1
Number of consecutive binarized values	6 to 10	LOW slot	HIGH slot
	14 to 18	LOW slot × 2	HIGH slot × 2
	22 to 26	LOW slot × 3	HIGH slot × 3
	30 to 34	LOW slot × 4	HIGH slot × 4

4.3 Tracking Method

4.3.1 State Transition Diagram

Figure 4.14 shows a state transition diagram for tracking. The state transitions are divided into initial transitions and normal transitions.

In the initial state, a beacon light is searched using a wide view in state (1). If a beacon is found, the state transits to state (2) and the system controller attempts to demodulate a station ID from the beacon light using a narrow view image. If the demodulation of a station ID fails, or if the station ID is the same as its own ID, the state transits to state (1) and the system controller searches for a beacon light in the wide view. If the demodulation of a station ID succeeds and the station ID is correct, the state transits to the normal transition.

In the normal transition, handover processing is performed in state (3) firstly. After the handover is completed, the state transits to state (4) for tracking using a narrow view image. During the tracking, a new beacon is always checked in the wide view.

If a beacon light is missed during tracking, the state transits to state (5). If the beacon light is rediscovered within a few frames, the state transits to state (4) again. Otherwise, a beacon light is always searched in the wide view. When a beacon light is found, a station ID is demodulated using the narrow view in state (6). If the station ID is not correctly demodulated,

the state transits to state (5). If the ID is correctly demodulated, the state transits to state (3), where handover process is performed.

If a beacon light is found on the wide view in state (4), the station ID is demodulated using the narrow view image in state (7). If the station ID is not correctly demodulated, the state transits to state (4). If the ID is correctly demodulated, the state transits to state (8), where handover is decided. In state (8), the system controller checks whether the newly found station ID indicates the correct ground station to be handover next. If not, the state transits to state (3), otherwise the state transits to state (4), the tracking process.

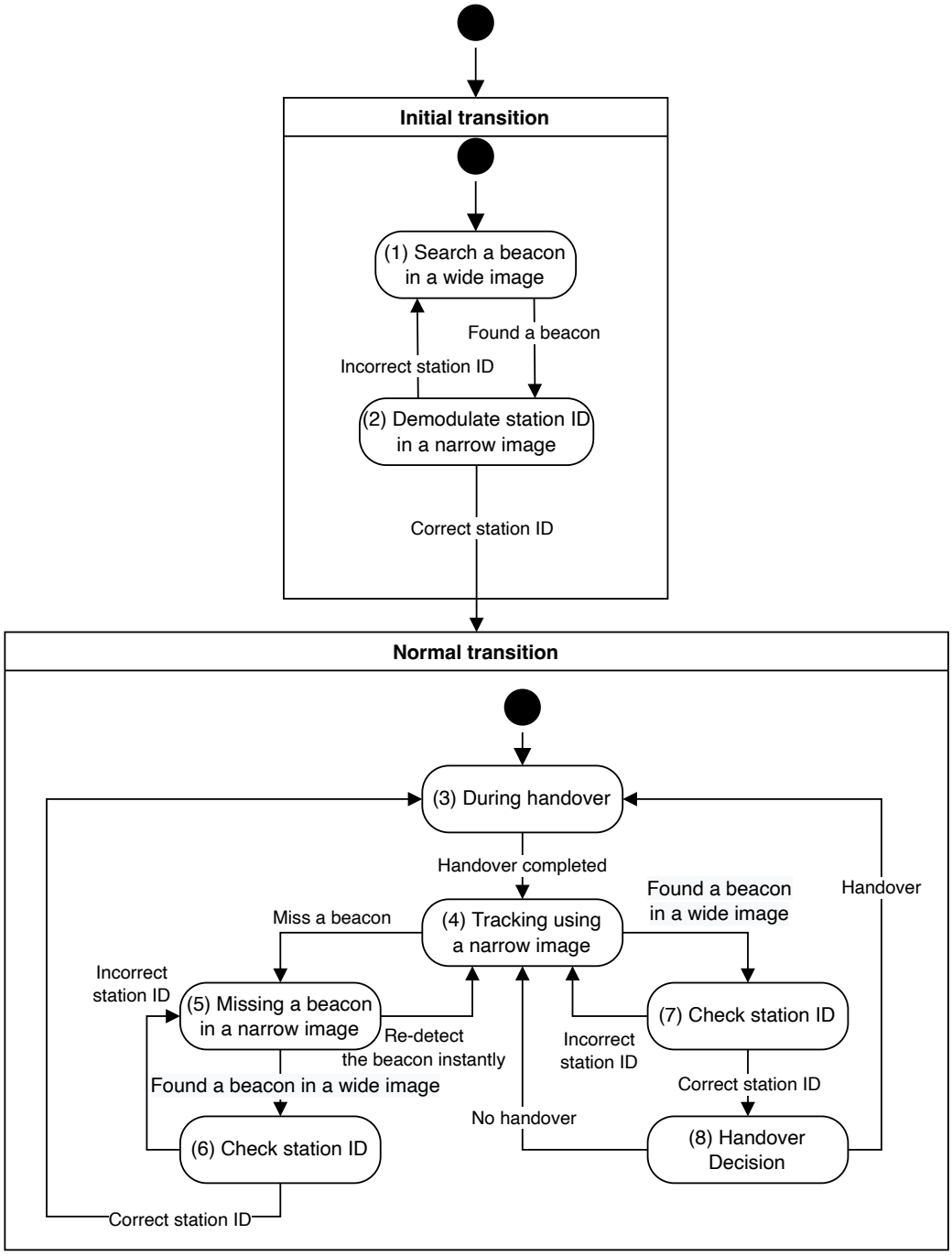

Figure 4.14: State Transition Diagram.

4.3.2 Beacon Tracking

In beacon tracking using the narrow view, the difference image of the latest two narrow view images is generated constantly. The difference image is binarized with a predetermined threshold value for labeling, and labeled with a labeling algorithm to determine a position of a beacon. The difference image is used to remove noise such as reflected light from the station's beacon and sunlight, same as in the case of the wide view. The threshold value for labeling used for binarization is obtained through prior experimentation. The beacon is the labeled area with the largest area. The center of gravity is calculated as a weighted average of the intensities. The beacon is tracked toward the center of the beacon.

During tracking the beacon, the position of the narrow image keep changing to the beacon be always in the center of the image. When the beacon's center approaches the edge of the image, the position of the narrow view image is shifted to the beacon be positioned in the center of the narrow view image.

4.3.3 Handover

If the station ID demodulated from the newly founded beacon is correct, the state transits to the handover process. First, the beacon position is reacquired from the latest narrow view image. Then, based on the calibration results, Windows PC calculates the mirror angle from the beacon position

in the image and drives the mirror actuator. After the handover, the state transits to tracking using a narrow view images.

4.4 Evaluation

4.4.1 Evaluation Environment

Two grand stations and a single mobile station were used in the experiments for evaluation in the Yagami Campus of Keio University (Yagami) on July 29, 2022 and in a test course in JARI (Japan Automobile Research Institute) [28] in Ibaraki Prefecture on October 13, 2022. Figures 4.15 and 4.16 show experimental scenes in Yagami and in JARI, respectively. Figure 4.17 shows the positions of the two ground stations and the mobile station in both experiments. The mobile station was mounted on a car instead of a train. An experiment at 5 km/h was conducted in Yagami. Experiments at 20 km/h, 30 km/h, and 40 km/h were conducted in JARI. This is because the road in Yagami is unsafe from an accident and too short for experiments at faster than 5 km/h. The performance around the handover was measured. The distance between the ground stations was approximately 30 m, and the car ran approximately 2 m away from the roadside where the ground stations were located. The `ping` command was used to measure disruption time during handover once at each speed (5 km/h, 20 km/h, 30 km/h, and 40 km/h). The `iperf3` command was used to measure throughput during handover once at 5 km/h, 20 km/h, and 30 km/h while three times at 40

km/h. The experiments in Yagami were conducted around 15:00 under clear sky. The experiments in JARI were conducted between 11:00 and 15:00. The weather was drizzling on and off. The road surface in Yagami was slightly bumpy. The road surface in JARI was smooth.

Figure 4.18 shows the network configuration for these experiments. The two ground stations are connected to a server PC on the ground side, and the mobile station is connected to a client PC on the car side. The client PC and server PC can communicate with each other without changing their IP addresses regardless of which ground station the mobile station is communicating with.

The 4 $\times$ 4 array of the beacon emitters was used in all the ground / mobile stations In this setting, the beacon light can reach as far as 45 m, which is longer than the distance between the mobile station and the ground station (less than 10 m) when the mobile station hands over to the ground station

4.4.2 Disruption Time due to Handover

When the mobile station finds a new beacon light, it tries to demodulate a station ID modulated in the new beacon light. If the demodulation is successful, the mobile station starts the handover procedure. The number of lost packets was measured by the `ping` command at a 1 ms interval between the client PC and the server PC in the test network shown in Fig. 4.18.

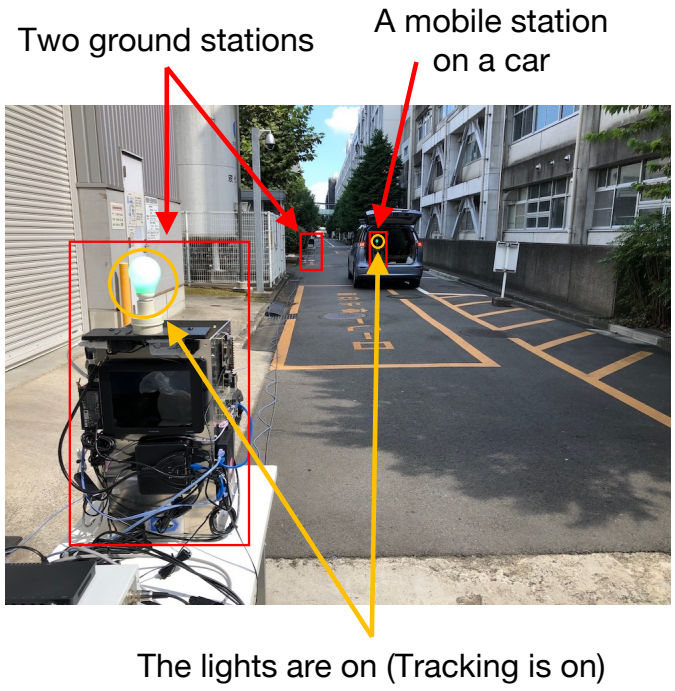

Figure 4.15: Environment at Yagami campus.

The results at all the speeds are shown in Table 4.7. Figure 4.19 shows the results at 40 km/h, which is typical of the experimental results. As shown in Table 4.7, only a single packet was lost around the handover. This indicates that the disconnection time in Layer-2 was less than 1 ms and the mirror rotation time during the handover was less than 2 ms. On the other hand, the disruption time was around 23 to 31 ms in LTC14 [12]. Thus, LTC22 substantially improves the disruption time due to handover compared to LTC14.

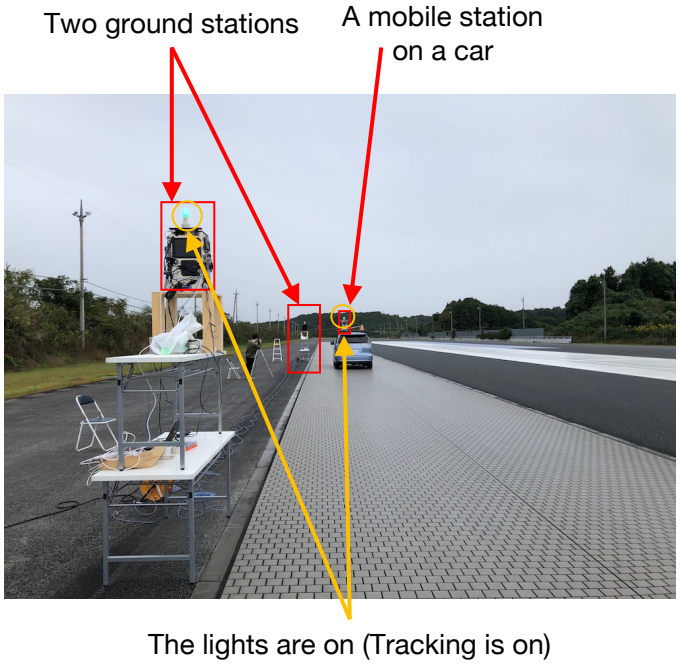

Figure 4.16: Environment at JARI.

4.4.3 Throughput during Handover

The `iperf3` command was used to measure the throughput at a 100 ms interval during handover. The `iperf3` server was started on the server PC in the test network shown in Figure 4.18. The `iperf3` client started on the client PC when the mobile station started communication with the first ground station.

The results at all the speeds are shown in Table 4.7. Figure 4.20 shows the results at 40 km/h, which is typical of the experimental results. As a result, the throughput around handover was approximately 94 Mbps. During

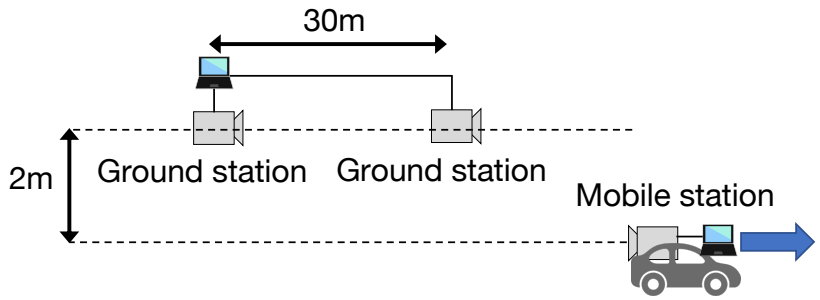

Figure 4.17: Evaluation environment.

Table 4.7: Experimental results.

Speed of the car	**Disruption time due to handover**	**Throughput during handover**
5 km/h	1 ms	89.3 Mbps
20 km/h	1 ms	77.5 Mbps
30 km/h	1 ms	77.6 Mbps
40 km/h	1 ms	75.3 Mbps

the handover, the throughput only decreased to approximately 89.4 Mbps. This means that the throughput decreased by approximately 5% during the handover. The throughput was measured every 100 ms, so it's assumed that communication was lost for approximately 5 ms (5% of 100 ms). The reason why the disconnection time in the `iperf3` command is longer than that in the `ping` command is considered that the packet size of the `iperf3` command is larger than that of the `ping` command. The throughput around handover was not measured in LTC14.

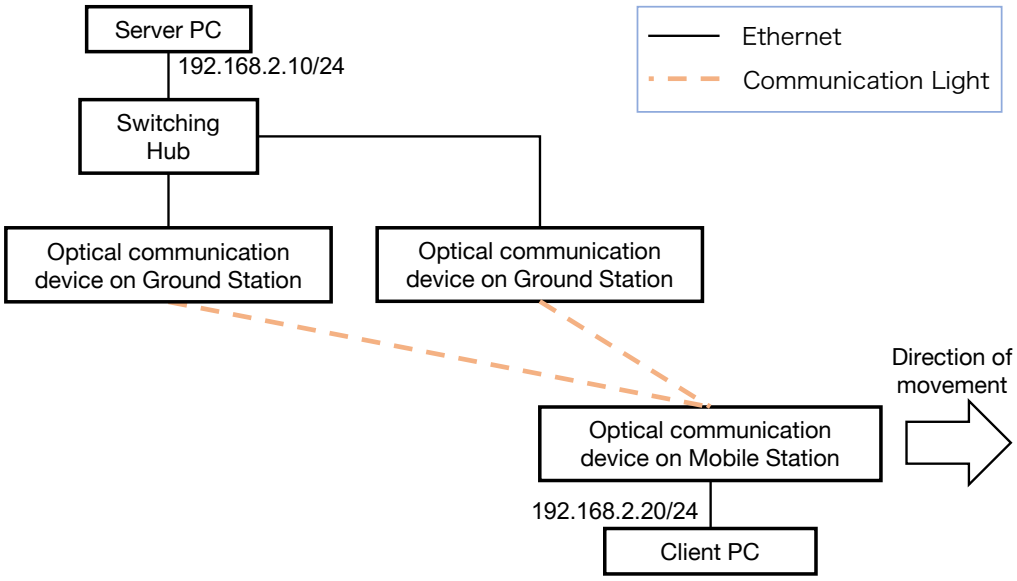

Figure 4.18: Evaluation network.

Figure 4.19: Result of ping command for 1 seconds around handover at 40 km/h.

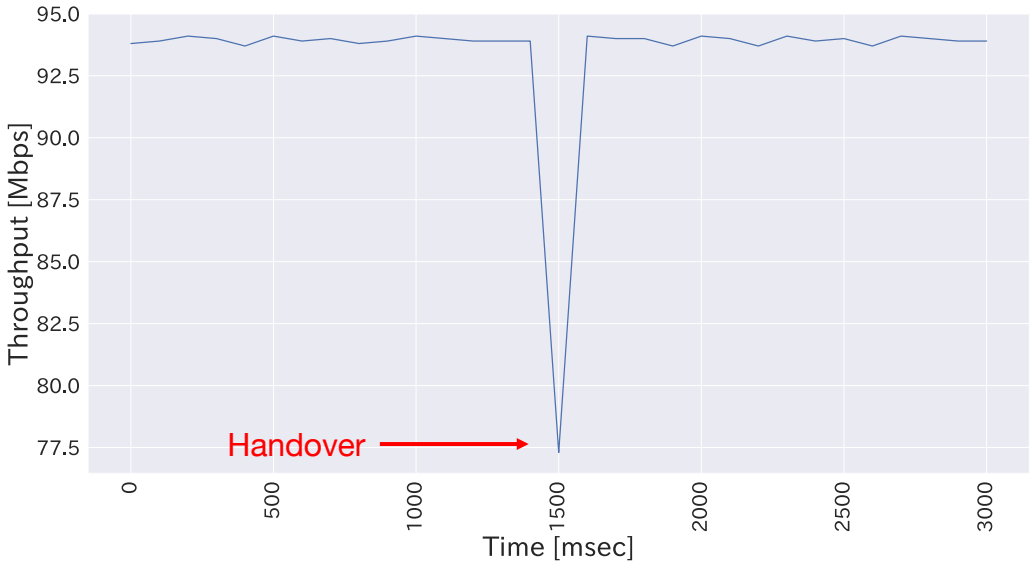

Figure 4.20: Throughput for 3,000 milliseconds around handover at 40 km/h.

Chapter 5

Discussion

5.1 Suitability for Real Environment

The suitability of the LTC22 system for a real environment is discussed. In the experiments, the speed of the car was 40 km/h at maximum and the distance between the ground stations was 30 m. Thus, the handover interval was 2.7 seconds at minimum. The communication speed was 100 Mbps. In a real environment, it can be assumed that the speed of the train will be 300 km/h or 500 km/h, the distance between the ground stations will be 300 m, and the communication speed will be 10 Gbps or higher.

The distance between the ground stations in the experiments (30 m) was decided considering the communication range of the 100 Mbps communication device and a margin. Since the communication range of the 10 Gbps communication device will be 500 m according to the vendor (Toyo Electric Corporation), the distance between the ground stations will be 300 m con-

sidering a margin in a real system. Thus, the handover interval will be 3.60 seconds at 300 km/h or 2.16 seconds at 500 km/h, which is not different so much from the handover interval in the experiments (2.7 seconds). On the other hand, the distance between the ground stations affects the number of ground stations installed along the railway. Based on a study of the Tokaido Shinkansen tracks, the number of ground stations does not decrease so much even if the distance between the ground stations is longer than 300 m.

5.2 Impact of Demodulation Time

Next, the impact of the demodulation time of the station ID in the handover process is discussed. The demodulation process is composed of "moving the position of the narrow view", "storing narrow view images", "image processing", and "calculation of the station ID". The total demodulation time is 63 ms. As shown in Fig. 4.14, the tracking process stops during the demodulation process. In Fig. 5.1, the mobile station is communicating with the ground station 1 and just finds a new beacon light from the ground station 2 at the position x_1. The mobile station starts the demodulation process of the station ID of the ground station 2. During the demodulation process, the mobile station goes away from the ground station 1 and reaches the position x_2 without tracking the ground station 1. After that, the mobile station executes the handover process from the ground station 1 to the ground station 2. For successful handover, the communication between the mobile station and the ground station 1 must be kept when the mobile station reaches the

position x_2.

In Fig. 5.1, d_{GS} is the distance between the ground stations. d_1 is the distance between the ground station 2 at the position x_0 and the position x_1. d_2 is the distance between the position x_1 and the position x_2. θ_c is the view angle of the dual-port camera, which detects the beacon light. θ_1 is the angle of the communication light to the ground station 1 when the mobile station reaches the position x_1. When the mobile station reaches the position x_2, the angle of the communication light remains unchanged (θ_1) although the correct angle of the communication light to the ground station 1 is θ_2. θ_l is the beam angle of the communication light. In order to keep the communication between the mobile station and the ground station 1 at the position x_2, "$\theta_1 - \theta_2 < \theta_l/2$" must be hold.

In Fig. 5.1, the following three equations are hold:

$$d_1 \tan \frac{\theta_c}{2} = 2[m] \tag{5.1}$$

$$(d_{GS} + d_1) \tan \theta_1 = 2[m] \tag{5.2}$$

$$(d_{GS} + d_1 + d_2) \tan \theta_2 = 2[m] \tag{5.3}$$

θ_c is 30 degrees. d_1 is 7.46 m. The demodulation time is 63 ms. d_2 at 300 km/h or 500 km/h is 5.25 or 8.25 m, respectively. Table 5.1 shows the

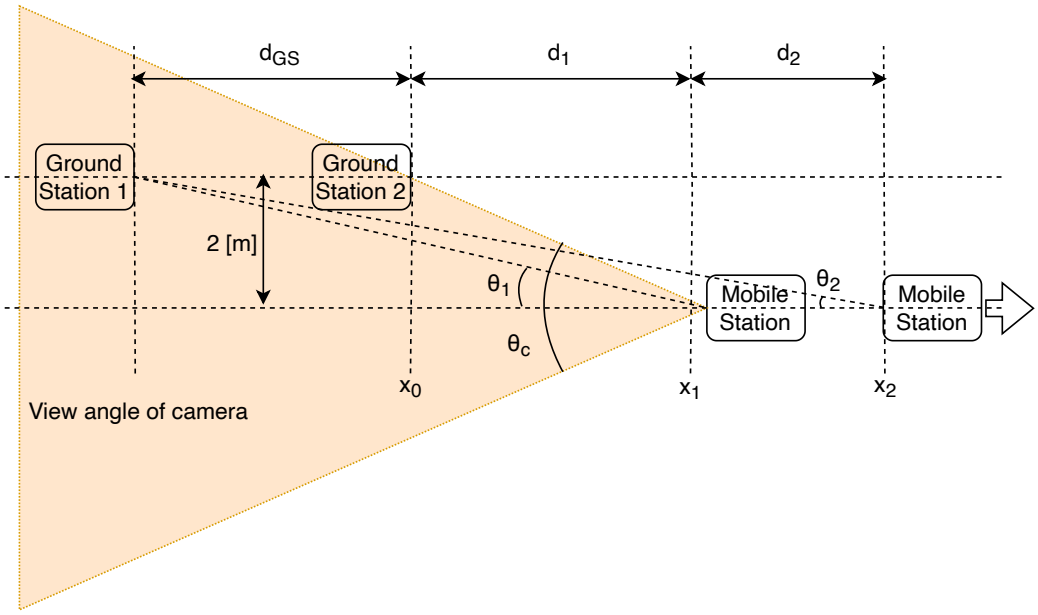

Figure 5.1: An example in which communication is not disrupted.

Table 5.1: $\theta_1 - \theta_2$ in various speeds and distance between ground stations.

Speed	$\mathbf{d_{GS}}$	$\mathbf{d_1}$	$\mathbf{d_2}$	$\boldsymbol{\theta_1 - \theta_2}$	**Remarks**
300 km/h	300 m	7.46 m	5.25 m	0.006 degrees	Shinkansen
500 km/h	300 m	7.46 m	8.75 m	0.01 degrees	Linear Shinkansen

values of "$\theta_1 - \theta_2$" in various speeds and distance between the ground stations. Since θ_l of the 10 Gbps communication device is 0.1 degrees according to the vendor, all the values are less than $\theta_l/2$ (= 0.05 degrees). Thus, it can be concluded that the demodulation time does not have bad impacts on the handover process.

Chapter 6

Conclusion

The Internet was originally designed as a wired network. With the emergence of mobile networks (e.g., in trains), network mobility has become a necessity. For a mobile network, mobility protocols and communication methods which can accommodate the movement of networks are required. And high-speed communication methods for mobile networks are still immature. The estimated throughput for a train in 2030 will reach 11 to 35 Gbps. Although cellular phone are available in a train, the cellular network becomes overloaded because of simultaneous handovers. Moreover, the throughput of the existing train networks is not enough. Millimeter wave communication for high-speed trains is still under research, and its throughput is less than 10 Gbps. In this context, free-space optical communication is proposed as a high-throughput communication method for train networks. Ground-to-train free-space optical communication technology has high throughput but tracking and handover have not been achieved. LaserTrainComm2012 (LTC12)

is one of the existing ground-to-train free-space optical communication systems, which employs a beacon light to notify the communication peer of its existence. LTC12, however cannot precisely find the location of the beacon light because LTC12 uses quadrant photodiode (QPD) to detect the beacon light.

In this dissertation, two new methods are proposed: rough tracking based on image recognition in an improved system called LaserTrainComm2014 (LTC14) and accurate tracking and handover based on a station ID in a new system called LaserTrainComm2022 (LTC22). In LTC14, rough tracking using a camera and precise tracking using a QPD were implemented. However, there are three problems such as unstable tracking due to analog control of a mirror actuator, overshooting caused by using a large mirror, and inability to identify stations. To solve these problems, LTC22 employed digital control of the mirror actuators, miniaturization of the mirrors, and station identification by modulating the station ID in the beacon light. As a result, a handover time is approximately 1 ms and TCP throughput of approximately 94 Mbps under normal conditions and 75-77 Mbps during handover.

There are three requirements to a ground-to-train free-space optical communication system in a real environment. First, the distance between ground stations should be more than 300 meters considering the shape of the railway of the Shinkansen and the number of the ground stations to be installed along the railway. It is planned that LTC22 is equipped with a 10

Gbps communication device although a 100 Mbps communication device is currently used in LTC22. The communication range of the 10 Gbps communication device is 500 m according to the vendor (Toyo Electric Corporation). Second, the system must be able to track and handover at a speed of 300 km/h (Shinkansen) or 500 km/h (Linear Shinkansen). LTC22 can theoretically track the communication peer and execute handover at a speed of 300 km/h or 500 km/h. Third, handover time in Layer-3 should be less than 310 ms. In LTC22, the handover time in Layer-2 is 1 ms, which is short enough for the requirement to the Layer-3 handover time.

For future work, improved LTC22 equipped with a 10 Gbps communication device should be developed and tested. Additionally, the vertical mirror actuator should be replaced with a new one which has the setting time as fast as that of the current horizontal mirror actuator (i.e., 390 µs). Finally, LTC22 should be miniaturized by downsizing the vertical mirror actuator and integrating the two horizontal mirrors.

References

[1] Cisco Systems, Inc. Cisco annual internet report (2018–2023) white paper. https://www.cisco.com/c/en/us/solutions/collateral/executive-perspectives/annual-internet-report/white-paper-c11-741490.html, March 2020.

[2] N. Abramson. Development of the alohanet. *IEEE Transactions on Information Theory*, 31(2):119–123, 1985.

[3] Pascal Thubert, Alexandre Petrescu, Ryuji Wakikawa, and Vijay Devarapalli. Network Mobility (NEMO) Basic Support Protocol. RFC 3963, January 2005.

[4] Kazuhiro Yamada. *A High Speed Mobile Communication System Implementing Bicasting Architecture on the IP Layer*. PhD thesis, Graduate School of Information Science and Technology, The University of Tokyo, August 2012.

[5] M. Aguado, O. Onandi, P. S. Agustin, M. Higuero, and E. J. Taquet. WiMax on Rails. *IEEE Vehhicular Technology Magazine*, 3(3):47–56,

September 2008.

[6] Hyoungjun Cho, Sungjin Shin, Goeun Lim, Changsung Lee, and Jong-Moon Chung. LTE-R handover point control scheme for high-speed railways. *IEEE Wireless Communications*, 24(6):112–119, 2017.

[7] Yong Chen, Kaiyu Niu, and Zhen Wang. Adaptive handover algorithm for LTE-R system in high-speed railway scenario. *IEEE Access*, 9:59540–59547, 2021.

[8] Nobuhide Nonaka, Kazushi Muraoka, Tatsuki Okuyama, Satoshi Suyama, Yukihiko Okumura, Takahiro Asai, and Yoshihiro Matsumura. 28 GHz-Band Experimental Trial at 283 km/h Using the Shinkansen for 5G Evolution. In *Proceedings of 2020 IEEE 91st Vehicular Technology Conference (VTC2020-Spring)*, pages 1–5, 2020.

[9] Shunsuke Takamatsu, Kosuke Mori, and Fumio Teraoka. Analysis of effects of periodical disconnection on streaming applications. IA2019-56 vol.119, no.343, IEICE Technical Report, December 2019. (in Japanese).

[10] H. Urabe, S. Haruyama, T. Shogenji, S. Ishikawa, M. Hiruta, F. Teraoka, T. Arita, H. Matsubara, and S. Nakagawa. High Data Rate Ground-to-Train Free-Space Optical Communication System. *Optical Engineering*, 51(3):031204–1–031204–9, March 2012.

[11] Kosuke Mori, Masanori Terada, Ryoji Murakami, Daisuke Yamaguchi, Kazuki Nakamura, Fumio Teraoka, and Shinichiro Haruyama. Fast Han-

dover Mechanism for High Data Rate Ground-to-Train Free-Space Optical Communication System. In *Proceedings of Globecom 2014 Workshop - Optical Wireless Communications*, pages 499–504, December 2014.

[12] Kosuke Mori, Masanori Terada, Daisuke Yamaguchi, Kazuki Nakamura, Kunitake Kaneko, Fumio Teraoka, and Shinichiro Haruyama. Fast Handover Mechanism for High Data Rate Ground-to-Train Free-Space Optical Communication Transceiver for Internet Streaming Applications. *IEICE Transactions on Communications*, E99-B(5):1206–1215, 2016.

[13] Kosuke Mori, Fumio Teraoka, and Shinichiro Haruyama. A Fast Handover Mechanism for Ground-to-Train Free-Space Optical Communication using Station ID Recognition by Dual-Port Camera. *IEICE Transactions on Information and Systems*, 2023. (accepted).

[14] A. Sniady and J. Soler. LTE for Railways: Impact on Performance of ETCS Railway Signaling. *IEEE Vehicular Technology Magazine*, 9(2):69–77, June 2014.

[15] Yuta Takahashi, Kazushi Muraoka, Jun Mashino, Satoshi Suyama, and Yukihiko Okumura. 5G Downlink Throughput Performance of 28 GHz Band Experimental Trial at 300 km/h. In *Proceedings of 2018 IEEE 29th Annual International Symposium on Personal, Indoor and Mobile Radio Communications (PIMRC)*, pages 1140–1141, 2018.

[16] Seung Nam Choi, Dukhyun You, Ilgyu Kim, and Dae Jin Kim. Uplink Design of Millimeter-Wave Mobile Communication Systems for High-

Speed Trains. In *Proceedings of 2014 IEEE 79th Vehicular Technology Conference (VTC Spring)*, pages 1–5, May 2014.

[17] Junhyeong Kim and Il Gyu Kim. Distributed Antenna System-based Millimeter-Wave Mobile Broadband Communication System for High Speed Trains. In *Proceedings of 2013 International Conference on ICT Convergence (ICTC)*, pages 218–222, October 2013.

[18] T. Yuge and S. Sasaki. Train Radio System Using Leaky Coaxial Cable. In *Proceedings of 34th IEEE Vehicular Technology Conference*, pages 43–48, May 1984.

[19] D.T. Fokum and V.S. Frost. A Survey on Methods for Broadband Internet Access on Trains. *IEEE Communications Surveys Tutorials*, 12(2):171–185, Second Quarter 2010.

[20] Atsushi Kanno, Pham Tien Dat, Toshimasa Umezawa, Naokatsu Yamamoto, Tetsuya Kawanishi, Nagateru Iwasawa, Nariya Iwaki, Kazuki Nakamura, Kunihiro Kawasaki, Naoki Kanada, Naruto Yonemoto, Yosuke Sato, Masato Fujii, Katsuya Yanatori, Nobuhiko Shibagaki, and Kenichi Kashima. Field trial of 1.5-gbps 97-ghz train communication system based on linear cell radio over fiber network for 240-km/h high-speed train. In *Proceedings of 2019 Optical Fiber Communications Conference and Exhibition (OFC)*, pages 1–3, 2019.

[21] Kjell Larsson, Bjoern Halvarsson, Damanjit Singh, Ranvir Chana, Jawad Manssour, Minsoo Na, Changsoon Choi, and Sungho Jo. High-

speed beam tracking demonstrated using a 28 ghz 5g trial system. In *Proceedings of 2017 IEEE 86th Vehicular Technology Conference (VTC-Fall)*, pages 1–5, 2017.

[22] E. Ciaramella, Y. Arimoto, G. Contestabile, M. Presi, A. D'Errico, V. Guarino, and M. Matsumoto. 1.28 terabit/s (32x40 Gbit/s) wdm transmission system for free space optical communications. *IEEE Journal on Selected Areas in Communications*, 27(9):1639–1645, 2009.

[23] M. Toyoshima, S. Yamakawa, T. Yamawaki, K. Arai, M.R. Garcia-Talavera, A. Alonso, Z. Sodnik, and B. Demelenne. Long-term statistics of laser beam propagation in an optical ground-to-geostationary satellite communications link. *IEEE Transactions on Antennas and Propagation*, 53(2):842–850, 2005.

[24] Alberto Carrasco-Casado, Koichi Shiratama, Phuc V. Trinh, Dimitar Kolev, Femi Ishola, Tetsuharu Fuse, Hiroyuki Tsuji, and Morio Toyoshima. Nict's versatile miniaturized lasercom terminals for moving platforms. In *2022 IEEE International Conference on Space Optical Systems and Applications (ICSOS)*, pages 213–217, 2022.

[25] autoevolution. Spacex to turn on laser communications for starlink satellites, reducing internet latency. https://www.autoevolution.com/news/spacex-to-turn-on-laser-communications-for-starlink-satellites-reducing-internet-latency-191180.html, June 2022.

[26] Abdelbaset S. Hamza, Jitender S. Deogun, and Dennis R. Alexander. Evolution of data centers: A critical analysis of standards and challenges for fso links. In *2015 IEEE Conference on Standards for Communications and Networking (CSCN)*, pages 100–105, 2015.

[27] Navid Hamedazimi, Zafar Qazi, Himanshu Gupta, Vyas Sekar, Samir R. Das, Jon P. Longtin, Himanshu Shah, and Ashish Tanwer. Firefly: A reconfigurable wireless data center fabric using free-space optics. In *Proceedings of the 2014 ACM Conference on SIGCOMM*, SIGCOMM '14, page 319–330, New York, NY, USA, 2014. Association for Computing Machinery.

[28] JARI: Japan Automobile Research Institute. Shirosato test center. https://www.jari.or.jp/test-courses/stc/, Jan 2023.

[29] Yuhei Hoashi. Speed-up and improving accuracy of the control of mirror actuator for free-space optical train-to-ground communication. Master's thesis, Graduate School of System Design and Management, Keio University, March 2019. (in Japanese).

[30] UMIP. http://www.umip.org, May 2018.

Appendix A

Structure of Control Software for LaserTrainComm2022

The source codes of the control software for LTC22 is stored in `https://github.com/TeraokaKanekoLab/LaserTrainComm`. Figure A.1 shows the structure of the source codes.

The source codes in the `zynq-vhdl` directory is a logic circuit on the Zynq board described in Sec. 4.1.6. The logic circuit handles the dual-port camera and pass the images to the Linux OS on the Zynq board via the DMA buffers. The logic circuit is written in `vhdl`.

The source codes in the `controller` directory is the software on the Linux OS on the Zynq described in Sec. 4.1.6. The software is written in `C++`.

The source codes in `actuator-canon` and `actuator-thorlabs` directories are the software running on the Windows OS described in Sec. 4.1.6

and control the horizontal actuator and the vertical actuators, respectively. The software on the Windows OS is written in `C#`.

The source codes in the `beacon-emitter` are the software running on the ESP32-WROOM-32 described in Sec. 4.1.6. The software controls the blink of the LED beacon emitter. The software on the ESP32-WROOM-32 micro computer is written in `Arduino language` based on `C++`.

Three LTC22 devices were developed in this dissertation: one for the mobile station and two for the ground stations. The configuration files (e.g., configs/*.conf, configs/*.json) in the `controller`, `actuator-canon`, and `actuator-thorlabs` directories are prepared for each LTC22 device because each LTC22 device has slightly different hardware characteristics.

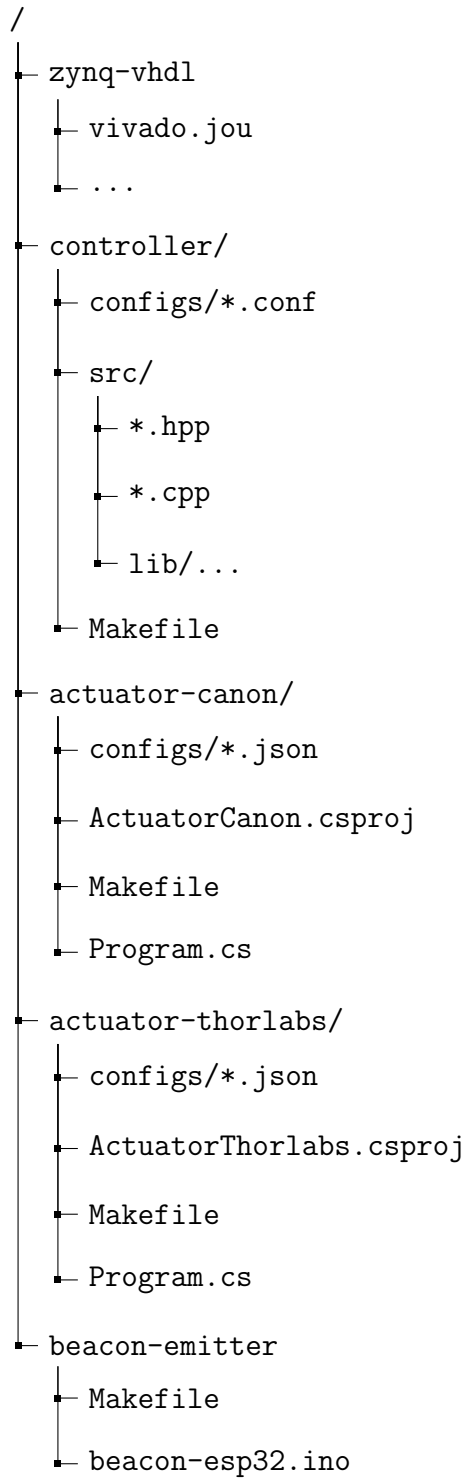

Figure A.1: Structure of source codes of LaserTrainComm2022.

Appendix B

Manual of LaserTrainComm2022

B.1 ESP32-WROOM-32 Micro Computer

The ESP32-WROOM-32 micro computer described in Sec. 4.1.6 is responsible for the control of the LED beacon emitter. The steps to set up the ESP32-WROOM-32 micro computer are as follows. A laptop PC in which `arduino-cli`, a command line interface, is already installed is required to configure the ESP32-WROOM-32 micro computer. The laptop PC is connected to the ESP32-WROOM-32 micro computer with a micro USB cable.

1. Launch a terminal emulator software in the laptop PC.
2. Move to the `beacon-emitter` directory described in Appendix A.
3. A sample station ID is already written in the `beacon-esp32.ico` file. Modify the station ID for an appropriate value. In practice, since the

three LTC22 devices are developed in this dissertation, the station IDs 1 to 3 are assigned to for each LTC22 device.

4. Run the following command to compile the program.

```
make build
```

5. Run the following command to upload the compiled program. `/dev/cu.usbserial-0001` is an example of the name of a USB-device in the laptop PC. Change the device's name to an appropriate value before running the command.

```
arduino-cli upload -p /dev/cu.usbserial-0001 \
    --fqbn esp32:esp32:esp32-poe-iso .
```

B.2 Windows OS

The Windows OS described in Sec. 4.1.6 is responsible for the receiving the position of the beacon light in an image from the system controller and controlling the horizontal and vertical actuators. The steps to set up the Windows OS as follows. The Windows OS and the mirror actuators are assumed to be already turned on and connected with cables. A laptop PC which is not described in Sec. 4.1.6 is used to access the Linux OS on the Zynq board and the Windows OS via the `ssh` command. The laptop PC is only used as a client of `ssh`.

1. Launch a terminal emulator software in the laptop PC and access the Windows OS via the `ssh` command.
2. Move to the `actuator-canon` directory described in Appendix A.
3. Run the following command to activate the software to control the horizontal actuator. "X" (1 to 3) is the serial number of the LTC22 devices in which the software is running.

   ```
   make startX
   ```

4. Launch another terminal emulator software in the laptop PC and access the Windows OS via the `ssh` command.
5. Move to the `actuator-thorlabs` directory described in Appendix A.
6. Run the following command to activate the software to control the vertical actuators. "X" (1 to 3) is the serial number of the LTC22 devices in which the software is running.

   ```
   make startX
   ```

Then the software for the horizontal and vertical actuators are ready to receive the position of the beacon light in an image from the system controller.

B.3 Linux OS on Zynq Board

The Linux OS on the Zynq board described in Sec. 4.1.6 is responsible for the receiving the position of the beacon light in an image from the system controller and controlling the horizontal and vertical actuators. The steps to set up the Linux OS on the Zynq board are as follows. As described in Appendix B.2, the laptop PC is used to access the Linux OS on the Zynq board via the `ssh` command.

1. Launch a terminal emulator software in the laptop PC and access the Linux OS on the Zynq board via the `ssh` command.
2. Move to the `controller` directory described in Appendix A.
3. Run the following command to activate the software to control the system controller. "X" (1 to 3) is the serial number of the LTC22 devices in which the software is running.

   ```
   make startX
   ```

Then the software for the Linux OS on the Zynq board begins to receive images from the dual-port camera via the DMA buffers and sends the position of the beacon light in the image to the Windows OS.

Appendix C

Measurement of Beacon Light's Observable Range

An experiment to measure the maximum beacon light's observable range was conducted on the riverside of Tamagawa River on July 27, 2018. Figure C.1 shows the LED beacon light emitter and Figure C.2 shows the dual-port camera for this measurement. In this experiment, LTC22 was under development. Therefore, the LED beacon light emitters and the dual-port camera were separated from the LTC22 devices. Figure C.3 shows the LED beacon light emitters seen from the location in which dual-port camera was placed.

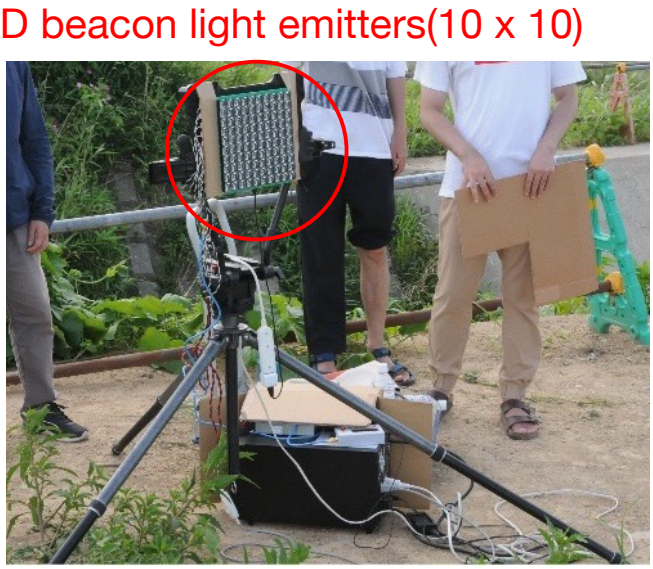

Figure C.1: LED beacon light emitters for the measurement of beacon light's observable range.

Figure C.2: Dual-port camera for the measurement of beacon light's observable range.

Figure C.3: LED beacon light emitters seen from dual-port camera.

The narrow view of the dual-port camera was used to detect the beacon light because the narrow view has less sensitivity than the wide view. This is because the exposure time of the narrow view is shorter than that of the wide view.

The distance between the dual-port camera and the beacon light emitters was 100, 200, 400, or 600 m. The number of the beacon light emitters was 2×2, 4×4, 8×8, or 10×10. The LED beacon light emitters were blinking at 4,000 Hz. The difference image was generated using the two successive narrow view images. The intensity of noise and the intensity of the beacon light in the difference image were measured.

Table C.1 shows the experimental results of the intensity of the beacon light or noise in the difference image. When the distance was 600 m, the beacon light was not detected in the difference image. Since the intensity of the beacon light should be higher than the intensity of noise (75), 4 x 4 was selected as the number of beacon light emitters at 400 m as the maximum distance.

Table C.1: Experimental result: The intensity of beacon light or noise in the difference image.

		Distance between the LED beacon and the dual-port camera			
		100 m	200 m	400 m	600 m
Number of LED beacon	10 × 10	1522	284	141	N/A
	8 × 8	844	201	96	N/A
	6 × 6	654	103	100	N/A
	4 × 4	362	76	81	N/A
	2 × 2	103	102	59	N/A
	Noise	90	60	75	75

Appendix D

Calibration

For tracking beacon, the relationship between the beacon's position in the image and the angle of the mirror is calculated in advance [29]. A 3D view of the actuators is shown in Fig. D.1. For simplicity, only a single horizontal actuator is shown here. The vertical actuator shown in Fig. D.2 is rotated θ degrees from the Y axis shown in Fig. D.1. The horizontal actuator shown in Fig. D.3 is rotated α degrees from the X axis as shown in Fig D.1. The Rx communication light and the Tx communication light are assumed to be coaxial. The normal vector $\mathbf{N}$ of the mirror (the blue arrow shown in Fig. D.3) is expressed as follows:

$$\mathbf{N} = \begin{bmatrix} 1 & 0 & 0 \\ 0 & \cos\theta & \sin\theta \\ 0 & -\sin\theta & \cos\theta \end{bmatrix} \begin{bmatrix} 0 \\ 0 \\ -1 \end{bmatrix} = \begin{bmatrix} 0 \\ -\sin\theta \\ -\cos\theta \end{bmatrix} \tag{D.1}$$

The unit vector representing the axis of the mirror rotation is expressed as follows:

$$\begin{bmatrix} 1 & 0 & 0 \\ 0 & \cos\theta & \sin\theta \\ 0 & -\sin\theta & \cos\theta \end{bmatrix} \begin{bmatrix} 0 \\ -1 \\ 0 \end{bmatrix} = \begin{bmatrix} 0 \\ -\cos\theta \\ \sin\theta \end{bmatrix} \tag{D.2}$$

According to the Rodoriguez's rotation formula, the normal vector $\mathbf{N}$ rotated α degrees around the unit vector (D.2) is expressed as follows:

$$\begin{bmatrix} \cos\alpha & \sin\theta\sin\alpha & \cos\theta\sin\alpha \\ \sin\theta\sin\alpha & \cos\alpha + \cos^2\theta(1-\cos\alpha) & -\cos\theta\sin\theta(1-\cos\alpha) \\ -\cos\theta\sin\alpha & -\sin\theta\cos\theta(1-\cos\alpha) & \cos\alpha + \sin^2\theta(1-\cos\alpha) \end{bmatrix} \begin{bmatrix} 0 \\ -\sin\theta \\ -\cos\theta \end{bmatrix} = \begin{bmatrix} -\sin\alpha \\ -\sin\theta\cos\alpha \\ -\cos\theta\cos\alpha \end{bmatrix} \tag{D.3}$$

In Fig. D.1, the vector $\mathbf{F} = \begin{bmatrix} 0 \\ 1 \\ 0 \end{bmatrix}$ is the unit vector of the communication light. The vector $\mathbf{F}$ is reflected by the mirror. The vector $\mathbf{R}$ represents the communication light reflected by the mirror, which is expressed using the vector $\mathbf{F}$ and the vector $\mathbf{N}$ as follows:

$$\mathbf{R} = \mathbf{F} - 2(\mathbf{F} \cdot \mathbf{N})\mathbf{N} \tag{D.4}$$

Thus, the vector $\mathbf{R}$ is expressed by (D.1), (D.3), and (D.4) as follows:

$$\mathbf{R} = \begin{bmatrix} 0 \\ 1 \\ 0 \end{bmatrix} - 2(-\sin\theta\cos\alpha) \begin{bmatrix} -\sin\alpha \\ -\sin\theta\cos\alpha \\ -\cos\theta\cos\alpha \end{bmatrix} = \begin{bmatrix} -2\sin\theta\sin\alpha\cos\alpha \\ 1 - 2\sin^2\theta\cos^2\alpha \\ -2\sin\theta\cos\theta\cos^2\alpha \end{bmatrix} \tag{D.5}$$

In Fig. D.4, (x_c, y_c) is the position of the beacon light when the center of the image is the origin. f represents the focal length of the camera. Since the beacon should be on the vector $\mathbf{R}$, the following equation holds.

$$\begin{bmatrix} -2\sin\theta\sin\alpha\cos\alpha \\ 1-2\sin^2\theta\cos^2\alpha \\ -2\sin\theta\cos\theta\cos^2\alpha \end{bmatrix} = \frac{1}{\sqrt{x_c^2+y_c^2+f^2}} \begin{bmatrix} x_c \\ y_c \\ f \end{bmatrix} \tag{D.6}$$

Therefore, θ and α are expressed as follows:

$$\theta = \arctan \frac{y_c - \sqrt{x_c^2+y_c^2+f^2}}{f} \tag{D.7}$$

$$\alpha = -\arctan \frac{x_c}{\sqrt{\left(y_c - \sqrt{x_c^2+y_c^2+f^2}\right)^2 + f^2}} \tag{D.8}$$

In practice, there will be errors in θ, α, and f. Calibration was manually performed by activating the mirror to match the direction of the communication light and that of the beacon light. Figure D.5 shows an environment for the calibration. The distance between the LTC22 devices 1 and 2 was 100 m. Figure D.6 shows the photo of the actual environment. The LTC22 device 1 can be rotated horizontally and vertically. By rotating the LTC22 device 1, the positions of beacon light was adjusted to the nine positions in the wide view image in the LTC22 device 1. θ (the rotation angle of the vertical actuator) and α (the rotation angle of the horizontal actuator) in the LTC22 devices 1 and 2 are adjusted to ensure the link of communication

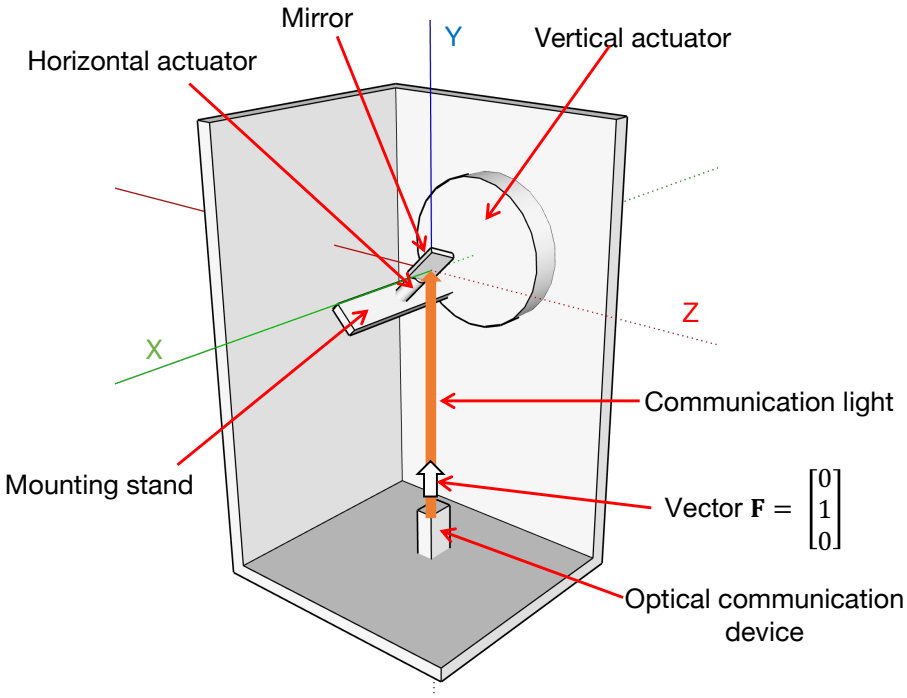

Figure D.1: 3D view of the device.

is up. Then, the beacon light's positions in a wide view image, θ and α, were measured for each beacon light position. The errors in θ, α, and f were corrected by using the result of this calibration.

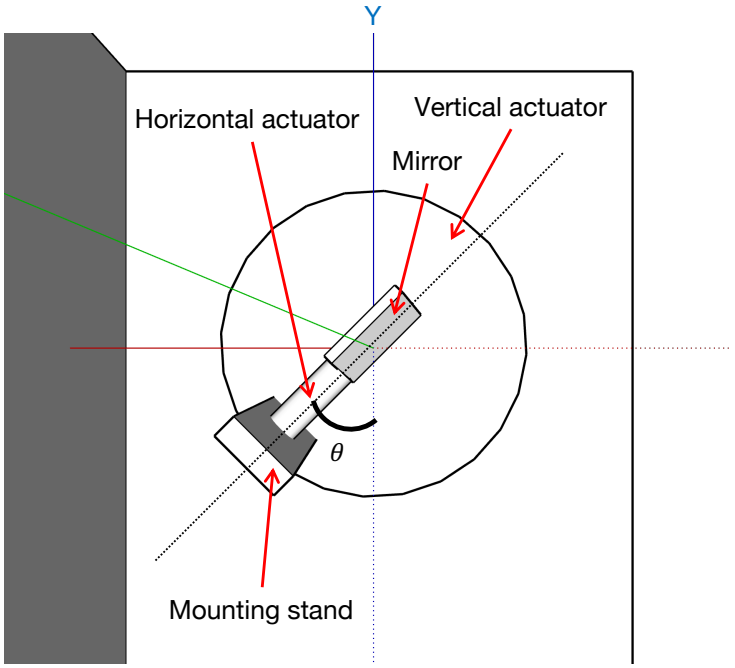

Figure D.2: Vertical actuator rotated θ degrees from Y axis.

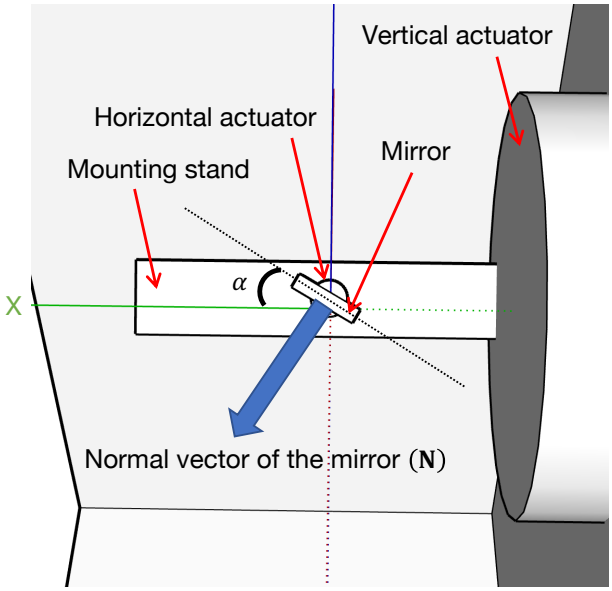

Figure D.3: Horizontal actuator rotated α degrees from X axis.

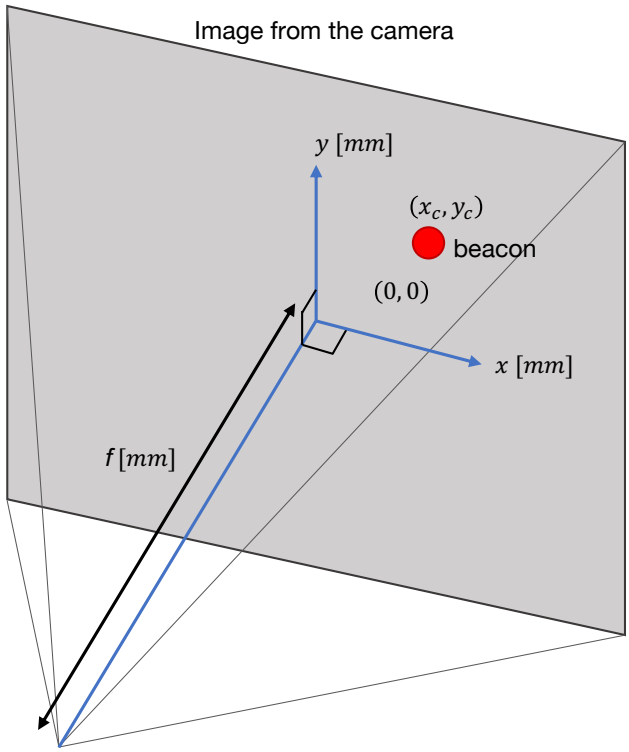

Figure D.4: (x_c, y_c) and f in the image.

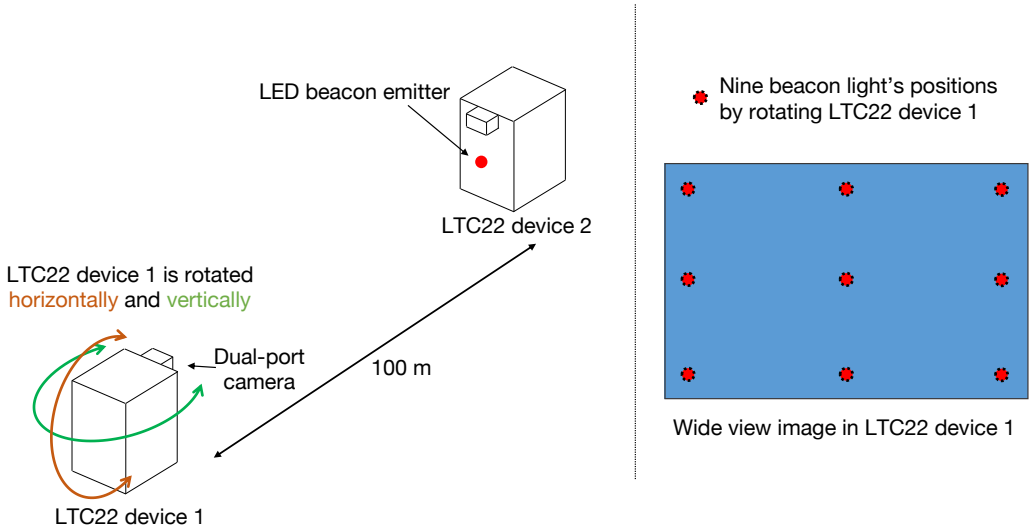

Figure D.5: Environment for calibration.

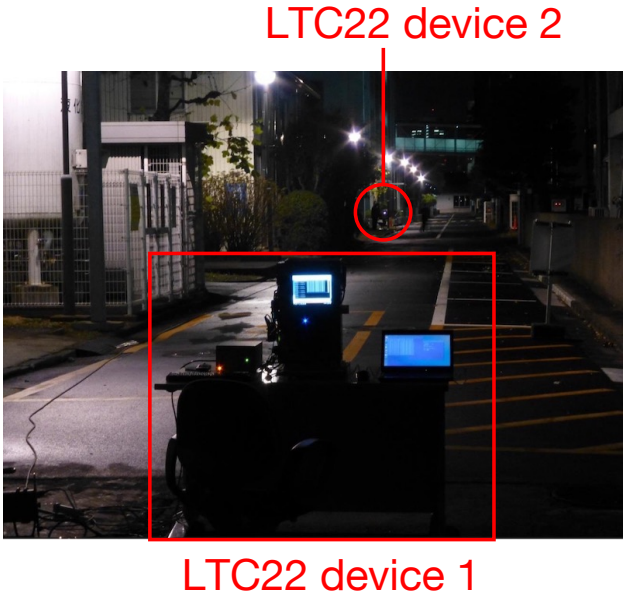

Figure D.6: Photo of calibration.

Appendix E

Emulation Environment of Network Mobility

Network mobility (NEMO) is required for ground-to-train communication in Layer-3 because the mobile station moves continuously and performs handover between ground stations.

Figure E.1 shows the NEMO environment in ground-to-train communication. The home agent and the mobile router are connected via IP-in-IP tunneling. Therefore, the mobile node can communicate with the correspondent node. If the mobile station moves and performs handover from the access router-1 to the access router-2, the mobile router send an information about new network of access router-2 to the home agent. Then, the IP-in-IP tunneling between the home agent and the mobile router is kept to be connected.

Figure E.2 shows the emulation environment of NEMO in ground-

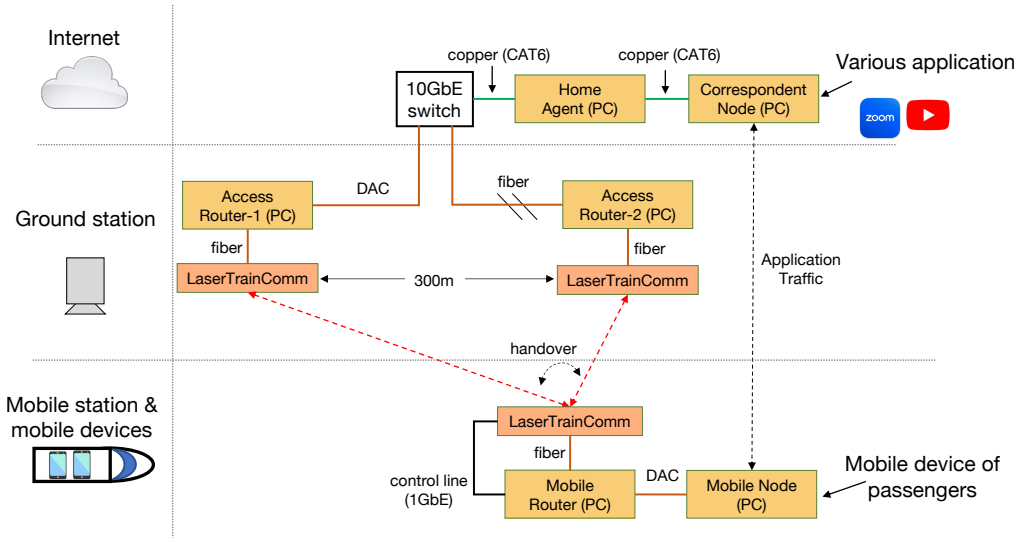

Figure E.1: Network mobility environment in ground-to-train communication.

to-train communication. Each node is a physical computer. Handover is emulated by an emulator which is a physical computer too. In practice, the emulator lets the link to the access router-1 down and lets the link to the access router-2 up to emulate handover. UMIP [30], an implementation of the NEMO basic support protocol [3], is used for this emulation. The time between the moment when the physical layer handover finishes and the moment when the NEMO signaling finishes was measured. Also the throughput and RTT between the mobile node and the correspondent node was measured.

Figure E.3 shows the result of the time of the NEMO signaling in Layer-3. Total time of the NEMO signaling in Layer-3 was $3.6+RTT_{MR-AR}+RTT_{MR-HA}$ ms. RTT_{MR-AR} represents the RTT between the mobile router

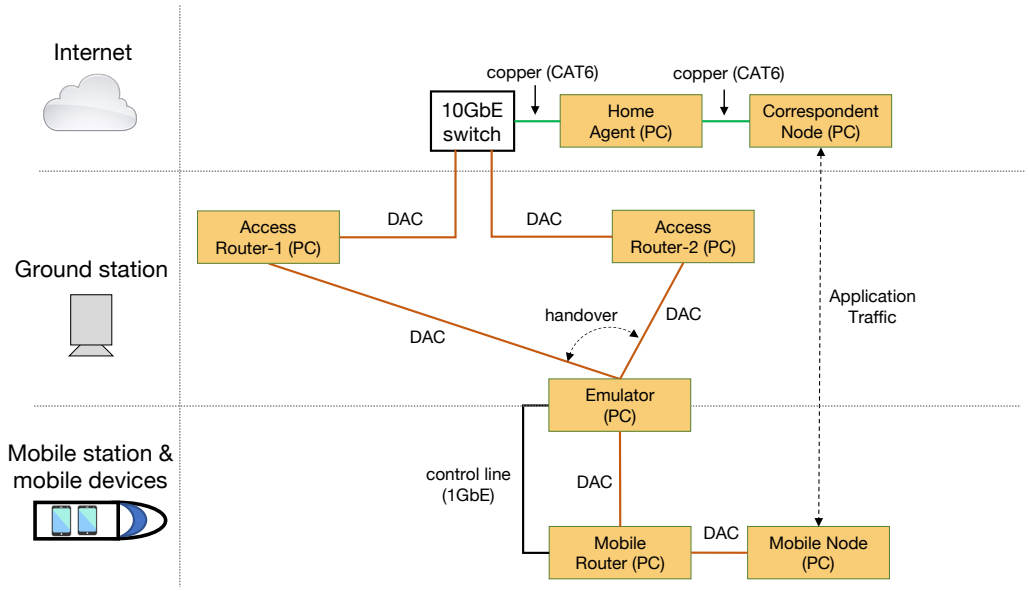

Figure E.2: Emulation environment of network mobility.

and the access router. RTT_{MR-HA} represents the RTT between the mobile router and the home agent. RTT_{MR-AR} and RTT_{MR-HA} are assumed to be less than 1 ms and several ms, respectively. Therefore, the total time of the NEMO signaling in Layer-3 should be less than 10 ms.

Table E.1 shows the throughput and RTT between the mobile node and the correspondent node. Both the throughput values with and without emulator were measured because the physical computer for the emulator did not have enough processing performance. With NEMO, the throughput was approximately 9 Gbps without emulator.

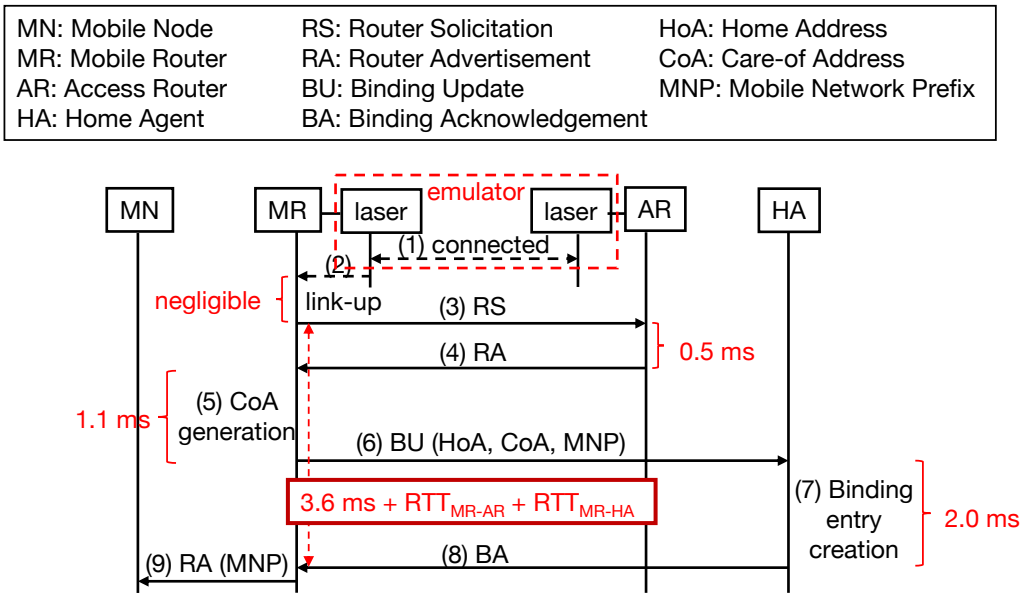

Figure E.3: Result of emulation: Signaling in Layer-3.

Table E.1: Throughput between the mobile node and the correspondent node.

		Protocol	Throughput	RTT
w/o NEMO	**w/o emulator**	TCP	9.31 Gbps	1.90 ms
		UDP	9.43 Gbps	
	w/ emulator	TCP	8.87 Gbps	2.35 ms
		UDP	9.21 Gbps	
w/ NEMO	**w/o emulator**	TCP	9.02 Gbps	1.96 ms
		UDP	8.61 Gbps	
	w/ emulator	TCP	7.70 Gbps	2.36 ms
		UDP	8.32 Gbps	

Appendix F

Dealing with Nose in Image of Dual-Port Camera

Striped noise was detected in a difference image generated from two successive narrow view images because of the specification of the dual-port camera. The stripe noise is shown on the upper side of Figure F.1. The positions of the striped noise must remain unchanged to remove the striped noise in the difference image. Due to the specification of the dual-port camera, the sizes of the narrow view and the wide view affect the position of the striped noise. After several trial, the sizes of the narrow view and the wide view were configured as shown in Table 4.1. The bottom side of Fig. F.1 shows the improved narrow view images and a difference image. The striped noise disappears in the difference image.

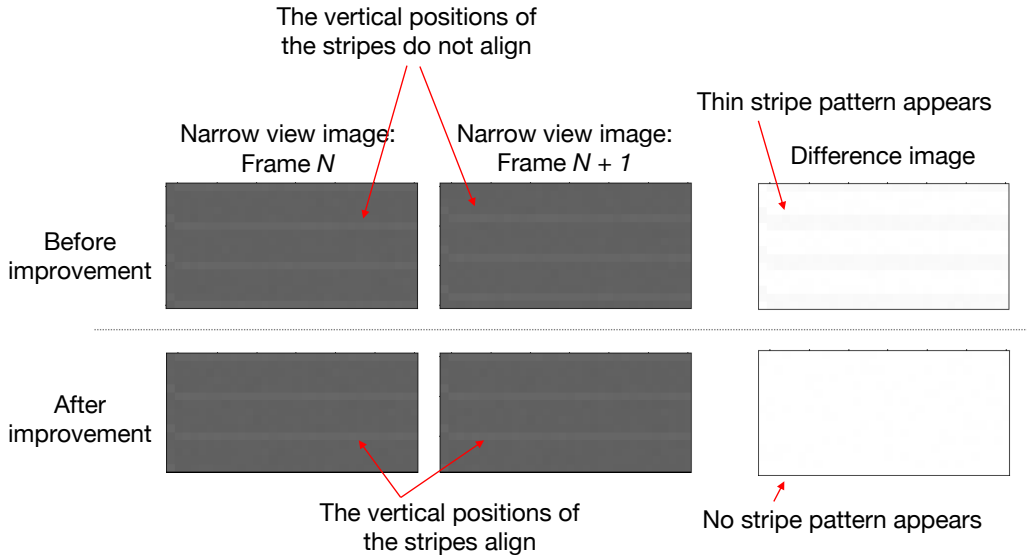

Figure F.1: Striped noise in a difference image.

Appendix G

Dealing with Interference between Communication Light and Beacon Light

Since the wavelengths of the communication light and the beacon light are approximately 860 nm and 950 nm, respectively, the close wavelengths cause interference that makes communication unstable. Figures G.1 and G.2 show optical spectrums of the beacon light and the communication light, respectively.

To avoid the interference, a 900 nm short-pass filter was attached at the light reception lens of the communication device to cut off the beacon light. Two filters are stacked to cut off the beacon light because only a single 900 nm short-pass filter is not enough to cut off the beacon light. Since the short-pass filter reflects light to be cut off, if the two filters are stacked in parallel, the light would reflect diffusely and filtering is not effective. There-

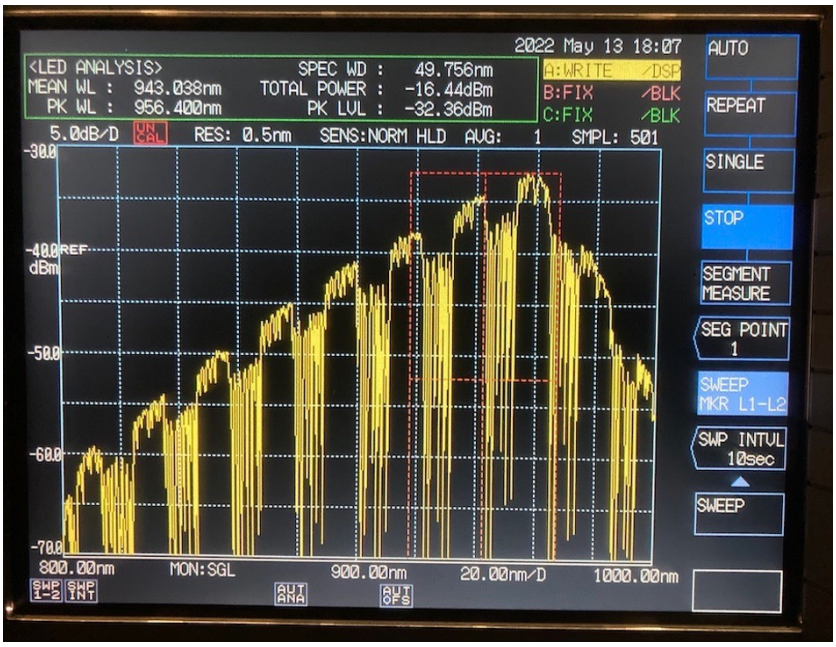

Figure G.1: Optical spectrum of beacon light.

fore, the two filters should diagonally be stacked at several angle. In this dissertation, two filters were stacked at a 30-degree angle. Figure G.3 shows the stacked two filters.

Figures G.4 and G.5 show optical spectrums of filtered beacon light and filtered communication light, respectively. Both optical spectrums are cut off at around 880 nm.

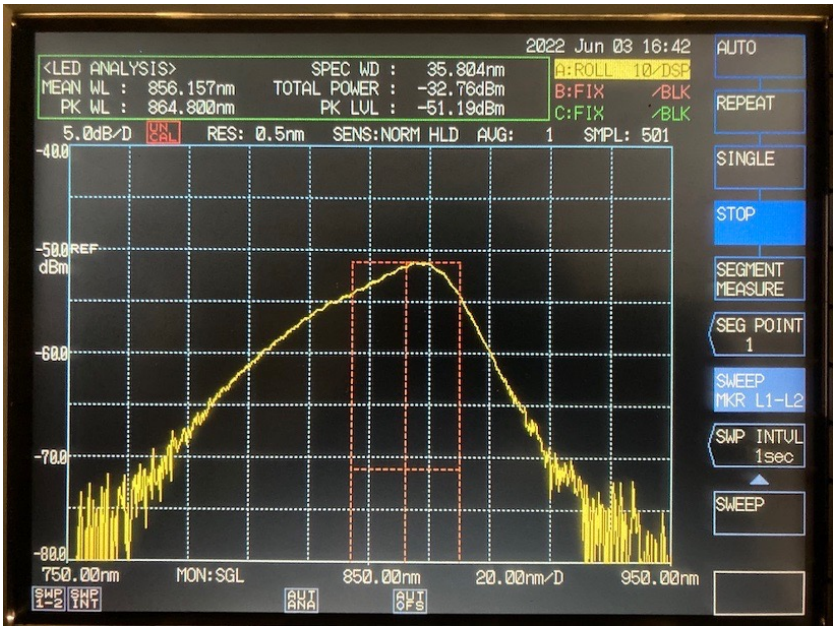

Figure G.2: Optical spectrum of communication light.

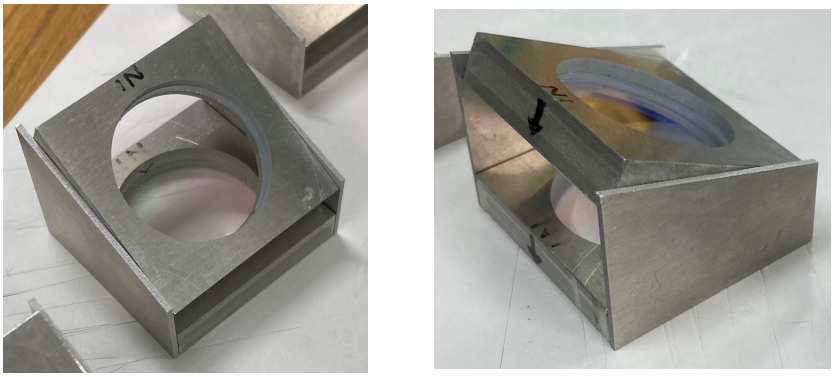

Figure G.3: Stacked two 900 nm short-pass filter at a 30-degree angle.

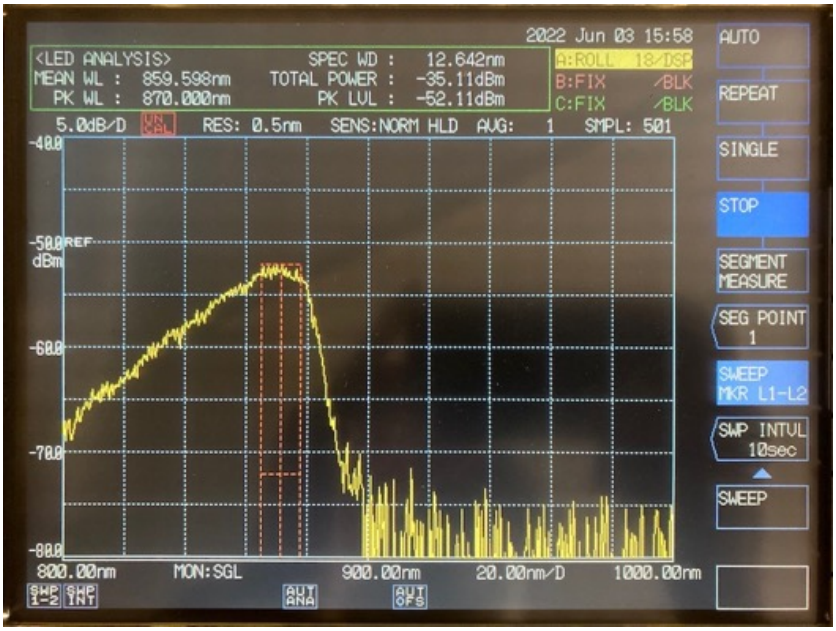

Figure G.4: Optical spectrum of filtered beacon light.

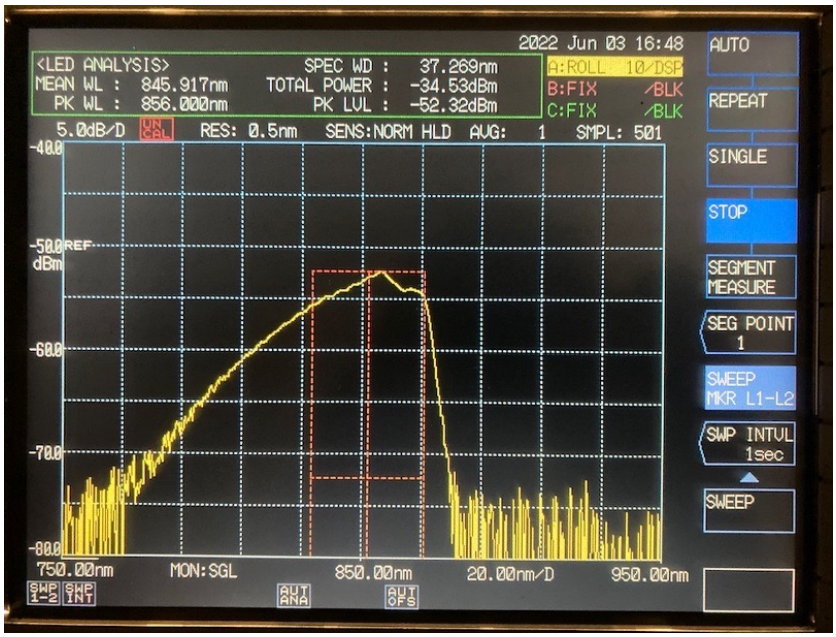

Figure G.5: Optical spectrum of filtered communication light.